Cavadas, F., Smith, I.F.C. and Figueiras, J. "Damage detection using data-driven methods applied to moving-load responses" Mechanical Systems and Signal Processing, Vol. 39, 2013, pp 409–425. doi 10.1016/j.ymssp.2013.02.019

Damage detection using data-driven methods applied to moving-load responses

Filipe Cavadas[a,*], Ian F. C. Smith[b], Joaquim Figueiras[a]

[a]*Laboratory for the Concrete Technology and Structural Behaviour (LABEST), Faculdade de Engenharia, Universidade do Porto, Rua Dr. Roberto Frias s/n, 4200-465 Porto, Portugal*

[b]*Applied Computing and Mechanics Laboratory (IMAC), School of Architecture, Civil and Environmental Engineering (ENAC), Ecole Polytechnique Fédérale de Lausanne, Station 18, CH-1015 Lausanne, Switzerland*

Abstract

Developed economies depend on complex and extensive systems of infrastructure to maintain economic prosperity and quality of life. In recent years, the implementation of Structural Health Monitoring (SHM) systems on full-scale bridges has increased. The goal of these systems is to inform owners of the condition of structures, thereby supporting surveillance, maintenance and other management tasks.

Data-driven methods, that involve tracking changes in signals only, are well-suited for analyzing measurements during continuous monitoring of structures. Also, information provided by the response of structures under moving loads is useful for assessment of condition.

This paper discusses the application of data-driven methods on moving-load responses in order to detect the occurrence and the location of damage. First, an approach for using moving-load responses as time series data is proposed. The work focuses on two data-driven methods – Moving Principal Component Analysis (MPCA) and Robust Regression Analysis (RRA) – that have already been successful for damage detection during continuous monitoring. The performance of each method is assessed using data obtained by simulating the crossing of a point-load on a simple frame.

Keywords: Bridges; Influence lines; Damage detection; Moving Principal Component Analysis; Robust Regression Analysis.

1. Introduction

Complex infrastructure systems ensure economic prosperity and quality of life. Therefore, maintaining civil infrastructure so that it is safe and reliable for daily use is important to all

* Corresponding author:
Tel.: (+351) 22 508 18 14; fax: (+351) 22 508 18 35
E-mail address: filipe.cavadas@fe.up.pt (F. Cavadas)

countries. However, existing infrastructure has suffered from decades of neglect and overuse, leading to accelerated deterioration of bridges, buildings, municipal and transportation systems, and resulting in a situation that has been described as "A global infrastructure crisis" [1]. Due to the age of existing bridges, increasing loads and changing requirements for use, maintenance and strengthening of bridges is becoming more and more important [2] [3] [4]. Often, the high costs of building new bridges are economically justifiable only through promise of longer service lives together with smaller maintenance costs compared with structures that are being replaced. Therefore, corrective maintenance of old structures is increasingly becoming a cost efficient alternative to the building of new structures [5].

Structural Health Monitoring (SHM) is a term that describes the use of a range of measurement systems on structures, including data interpretation.. The aim of these systems is to assist and inform owners of continued “fitness for purpose” of structures under gradual or sudden changes to their state and to learn about loading and response mechanisms [6]. SHM has potential to identify structural damage before it becomes critical, and thus represents a promising strategy in the ongoing challenge to achieve sustainable infrastructure [7].

Today, many bridges are monitored using sophisticated measurement systems employing hundreds of sensors. These systems generate large amounts of data and it is often difficult to detect early damage [8].There is thus a need for data interpretation techniques that provide reliable information to assist engineers in structural management. The choice and implementation of algorithms to process the data and carry out the identification is arguably the most crucial ingredient of a SHM system. Before choosing the data-interpretation algorithm, it is necessary to choose between two complementary approaches to the challenge: model-based (*inverse strategy*) or data-driven (*pattern recognition*) [9]. Model-based methods require the development of detailed numerical models of the structure. Measurements are compared with those predicted by the model with the aim of discovering anomalies in the behaviour of the structure. However, for civil infrastructure, creating such models is often difficult and expensive and this approach may not be successful in identifying the right anomaly. Data-driven methods consist of looking for changes in a “signature” of the structure that is related to its structural response under excitation. Anomalous behaviour is detected without information of physical processes requiring only initial conditions (no-anomalies) for training. Thus, these methods are generally faster than model-based methods as they do not require the evaluation of

computation-intensive numerical models. Strengths and weaknesses of both classes have been summarized in [10].

Since data-driven methods involve only tracking changes in signals, they are appropriate for analysing measurements during continuous monitoring of the performance of structures. Moyo and Brownjohn [11] applied the wavelet analysis and Omenzetter and Brownjohn [12] used Auto-Regressive Integrated Moving Average (ARIMA) models to identify events and changes in the structural state in a bridge. Lanata and Del Grosso [13] applied the Proper Orthogonal Decomposition (POD) to identify in time and locate in space the initiation of damage. Posenato et al. [14] presented two statistical methods: Moving Principal Component Analysis (MPCA) and Robust Regression Analysis (RRA) for damage detection during continuous static monitoring of civil structures. Through a comparative study with other statistical analyses they observed superior performance of these methods for damage detection.

Some methods have used the regular traffic responses to detect damage. Cardini and DeWolf [15] presented an approach based on determining the live load distribution factors for the girders, peak strains and the neutral axis locations from the strain data collected from normal truck traffic [16] to provide a continuous picture of the structural integrity of multi-girder steel bridges. Zaurin and Catbas [17] proposed a method in which video images and sensor data are correlated and used to create a series of unit influence lines (UIL) that are used as input features to detect and localize damage in the structure.

When periodic static loading tests are available, damage may be detected by comparing either the deflection curves or the influence lines of displacements and rotations before and after damage. Choi et al. [18] derived and proposed an *Elastic Damage Load Theorem* (EDLT) and demonstrated that the variations of the displacement reach the maximum at the damaged location independent of the location. Stohr et al. [19] showed that the differences between the influence lines of inclination measured under original and under modified structural conditions indicate clearly the existence and locations of stiffness changes. However, the application of these methods involves periodic static-load tests under controlled conditions, requiring the interruption of regular traffic. Furthermore, they imply knowing precise load levels used in the tests. Thus, in order to detect damage using influence-line data, development of other strategies is necessary.

This work presents an approach to perform damage detection based on moving-load data of regular traffic. The exact load level that is crossing the structure does not need to be known. The approach consists of applying two data-driven methods – MPCA and RRA – that have already been shown to be successful in continuous monitoring, to another type of data, influence-line information. It is worth noting that only the quasi-static component of the response is taken into consideration in the study. The objective is to detect and to localize the damage. Section 2 presents the framework and the approach adopted in order to use these two methods on influence-line data. In Section 3 the use of each method for SHM is briefly described. Using numerically simulated data, Section 4 presents the results obtained with each method.

2. Methodology

This section describes how influence-line data may be used for damage detection. The shape and magnitude of the influence line of a bridge load effect is representative of its static behaviour. However, the regular traffic response may contain a dynamic component. Dynamic components are particularly present in light-weight steel pedestrian bridges. In the case of a concrete medium-span bridge with smooth wear surface and joints, the dynamic component caused by a moving vehicle on the bridge response is generally negligible [20]. However, in some situations the dynamic component in the signal cannot be neglected. Therefore, the removal of the dynamic component of the signal prior to the application of this methodology is required. Paultre et. al [21] proposed the application of a digital low-pass filter to the measured time series whereas González and O'Brien [20] employed wavelet analysis to extract the total static component from the measured bridge response. Thus, considering these filtering techniques to remove the dynamic component of the signal, the present methodology takes into consideration the quasi-static response of the structure only. The damage detection procedure is illustrated by using a simple frame. The need for employing advanced methodologies to process the influence-line data obtained under different load levels is first demonstrated. Then, the approach proposed for using moving-load measurements for model-free interpretation is presented.

2.1. Description of the frame

The structure adopted to illustrate the employment of data-driven methods applied to moving-load responses for damage detection was a simple frame, 1.50 m high and 3.20 m long, as shown in Fig. 1. The elements are 0.50 m wide and 0.20 m thick. The geometry of the frame's

bases, 0.40 m long and 0.20 m thick, allow different positions for the supports. In normal operating conditions the supports are centred in the middle of the columns cross-section. The left support is a roller bearing, allowing horizontal displacements and rotations over the longitudinal direction. The right support is a pinned bearing, restraining the horizontal displacement but allowing the rotation over the longitudinal direction. Therefore, considering vertical loads only and ensuring this bearings configuration, the response of this frame is the same as that of a simply supported beam.

This structure was chosen because of planned future research involving the experimental validation of the methodology. Through simple modifications, the study of several structural systems is possible. The structural response of the frame for the support conditions described above is equivalent to that of a simply supported beam. However, by replacing the roller bearing by a pinned one, this structure becomes a concrete rigid-frame that resembles a bridge which is typically used for either overpasses or underpasses. In addition, under these support conditions, the beam's response is similar to that of the central span in a 3-span continuous beam. Finally, considering once again the support conditions and loading illustrated in Fig. 1, it may be viewed as a model of a beam where the distance of the support bearings to the longitudinal axis of the beam is amplified. This facilitates studies of bearing stiffness properties for investigations of the effects of bearing malfunction. Therefore, in the context of future research into the validation of this methodology in the laboratory as well as other studies, this very compact and versatile model enables testing of a wide variety of scenarios.

The response is assumed to be linear and elastic, where the Young's modulus has been assumed to be 15 GPa. This relatively low value was obtained through experimental testing. Using the numerical model, the structural response is estimated for a set of successive positions along the beam, which, for practical applications, is numerically equivalent to monitoring the structure while a point load moves across the frame at a slow speed. The results are presented graphically in the form of influence lines that represent the variation of response at a given point due to a load traversing the structure. As depicted in Fig. 1, the response of the structure is characterized through two displacements – the vertical deflection at mid-span (VDM) and the horizontal displacement at the roller support (HDR) – and two rotations – the rotation over the left support bearing (RLB) and the rotation over the right support bearing (RRB).

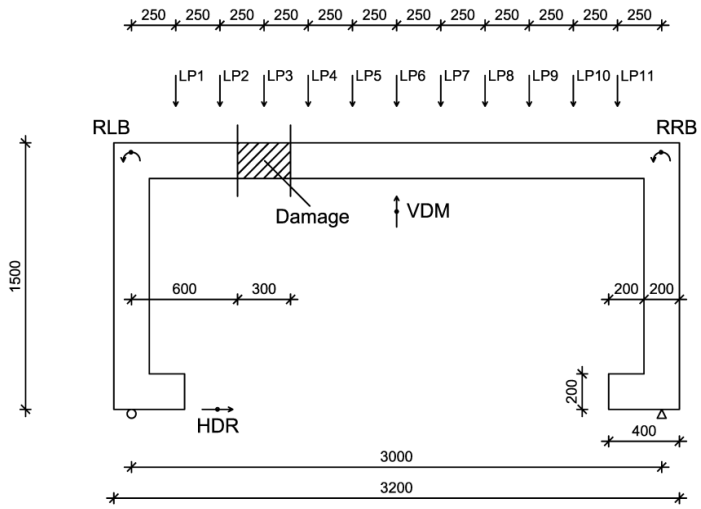

Fig. 1 – Frame model.

In order to make the study more realistic, noise was added to the simulated data. Sensor noise was assumed to have a uniform probability density function. The range, assumed to be ±0.01 mm for displacements and $\pm 1° \times 10^{-3}$ for rotations, is based on observations made during preliminary laboratory testing that was aimed at quantifying the precision of the sensors as well as ambient electrical noise.

2.2. The problem of detecting damage under different load levels

Consider a damage scenario corresponding to a local crack in a pre-stressed and reinforced concrete element. For the sake of simplicity it will be represented as a 20% stiffness reduction in a 30 cm length beam element, as depicted in Fig. 1. This damage scenario leads to an increase of 2% in the vertical deflection at mid span under a point load placed at mid-span. For example, under a service load of 8.75 kN, the vertical deflection varies from 1.00 mm to 1.02 mm before and after damage, respectively.

Comparing the responses, under a given load value, before and after the stiffness reduction both the occurrence and the location of the damage can be detected. As shown in the plots of Fig. 2 (left), since the influence lines obtained before (black) and after (gray) damage are slightly different, comparing them can be a means of detecting changes in the structural condition. However, the location of the damage remains unknown. Nevertheless, as shown in [18] and [19], computing the differences between the influence lines, allows the determination of the damage location, which corresponds to the position of the highest difference. As depicted in the plots of Fig. 2 (right), the position of the largest differences corresponds to the region of the stiffness reduction. However, if the load crossing the structure is not exactly the same before

and after the occurrence of damage, no significant difference may be noticed and, thus, the occurrence of damage may not be detected.

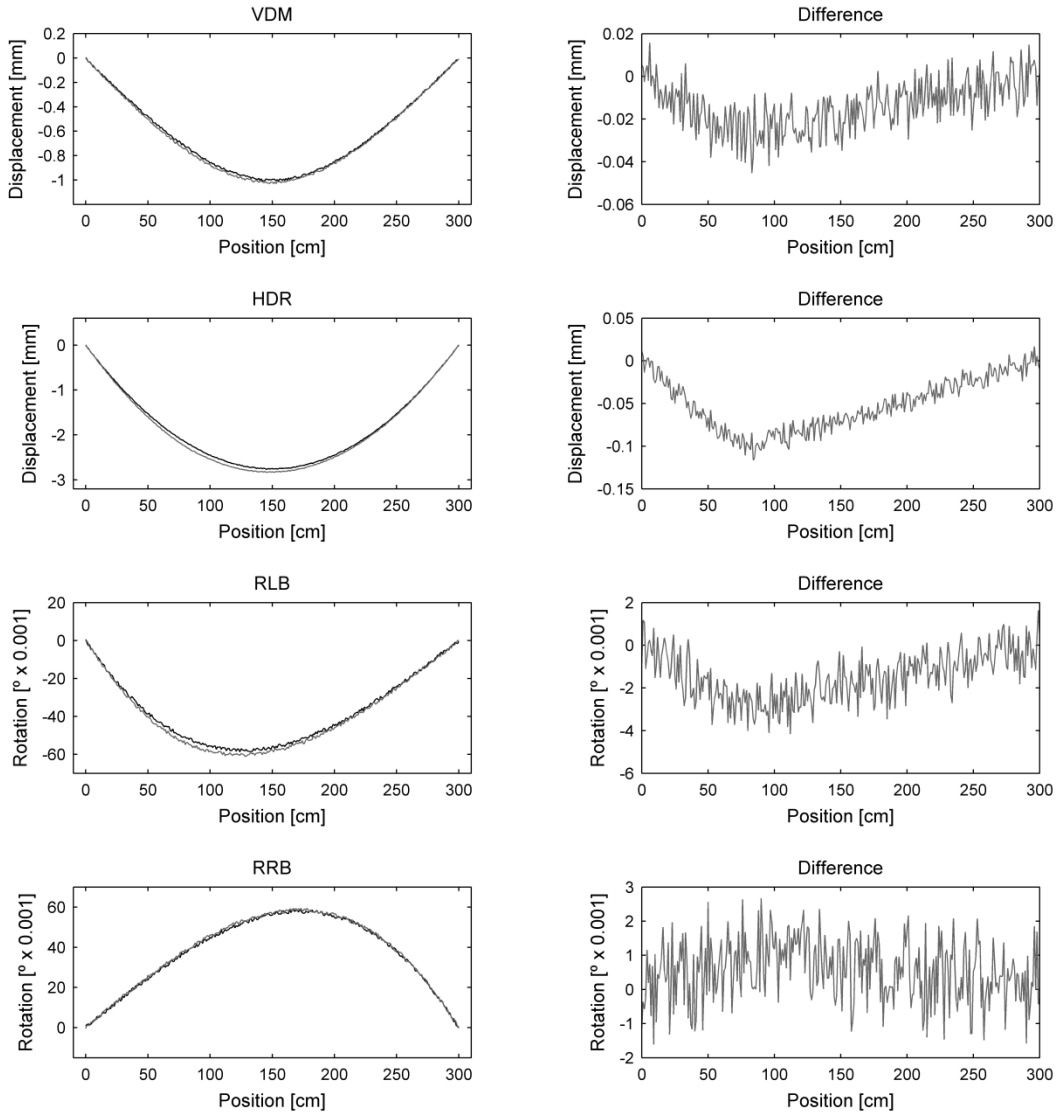

Fig. 2 – Comparison of the influence lines in the baseline condition (black) and in the damaged condition (gray), left, and the corresponding differences between the responses, right.

Consider, for example, that the uncertainty in quantifying the load is ±10%. Fig. 3 presents the responses of the structure: i) under the reference moving load (ML), before damage (black); ii) under 1.10xML, before damage (light gray); iii) under 1.07xML, after damage (gray). The difference between the influence lines for a load 10% higher than the reference load before damage and for a load 7% higher than the reference load after damage is negligible (Fig. 3, left). Furthermore, the difference between these influence lines and those obtained before damage under the reference load is also small (Fig. 3, right). Therefore, when the load cannot be quantified accurately, and thus, is uncertain, the occurrence of damage may not be detected.

Therefore, in order to detect the occurrence of damage using influence-line data, the application of another strategy is necessary.

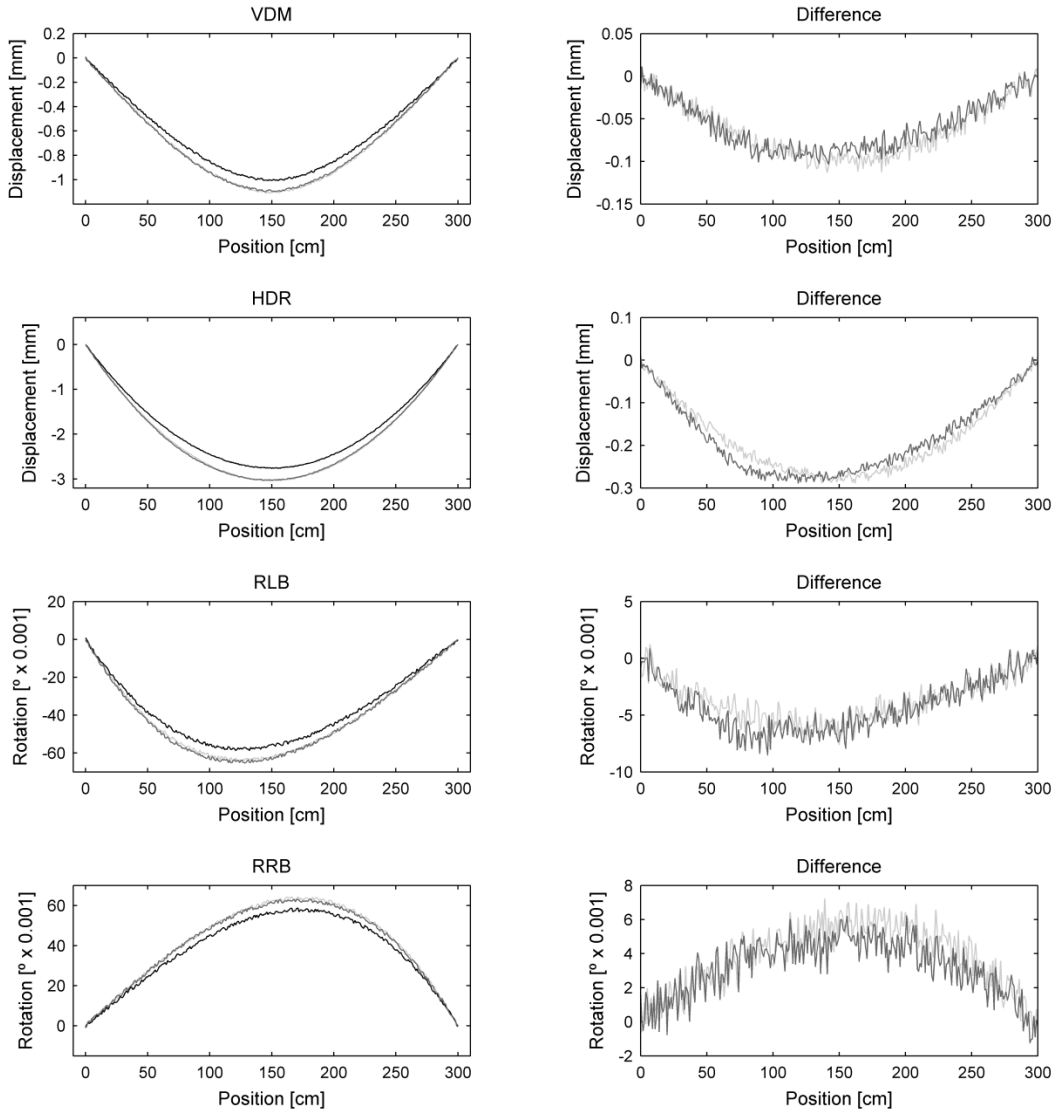

Fig. 3 – Comparison of the influence lines in the: i) baseline condition, under the reference moving load – ML (black); ii) baseline condition, under 1.10xML (light gray); iii) damaged condition, under 1.07xML (gray), left, and the differences between the responses ii-i (light gray) and iii-i (gray), right.

2.3. Model-free interpretation of moving-load measurements

The approach proposed in this paper regarding the application of data-driven methods to detect damage involves building time series using moving-load data. Consider a period in which n passages of vehicles were recorded and, in each passage, the response at m equally spaced points was recorded. Two types of time series – type I and type II – can be built.

A time-series type I involves the whole influence line. Whenever a load crosses the structure its response is collected and recorded in a time series that includes the previous crossings, leading to a time series containing l measurements, in which $l = n \times m$. The i^{th} measurement in the

time series corresponds to the value recorded at the q^{th} position on the structure during the k^{th} passage, as expressed in equation (1):

$$i = (k-1) \times m + q \tag{1}$$

Fig. 4 presents a time series containing 29 influence lines ($n = 29$) of the vertical displacement at mid-span (VDM), under a load uncertainty of ±10%, ranging from 0.90 to 1.10 times a service load of 8.75 kN, according to a uniform probability density function. Each influence line involves 301 measurements ($m = 301$), leading to a total of 8729 observations.

A time-series type II involves the response at a given load position (LP) for the successive crossings. Therefore, each time series contains n measurements. Based on the response recorded by each sensor one can build as many time series as the number of load positions considered for the data acquisition. In Fig. 5 the time series of the vertical displacement at mid-span (VDM) when the load was also at mid-span, load position 6 (see Fig. 1), is presented. Note that this time series is based on the same data presented in Fig. 4.

Using these two types of time series, the damage detection procedure will be carried out using two data-driven methods: Moving Principal Component Analysis (MPCA) and Robust Regression Analysis (RRA).

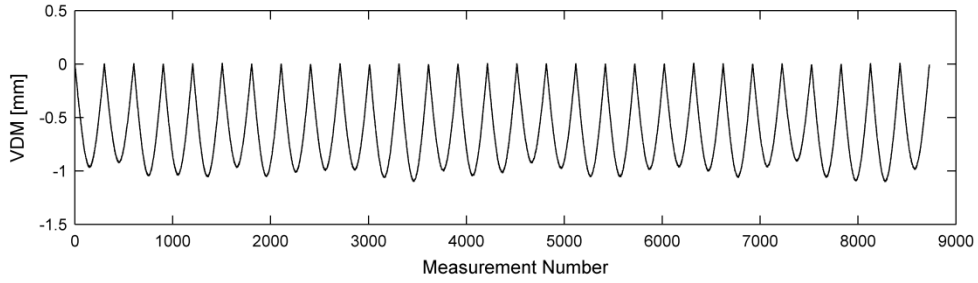

Fig. 4 – Time-series type I, of the vertical displacement at mid-span (VDM).

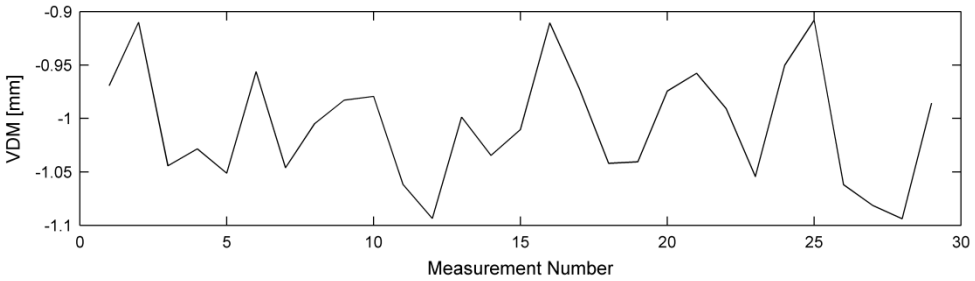

Fig. 5 – Time-series type II, of the vertical displacement at mid-span (VDM) when the load is at mid-span, LP6.

3. Data Interpretation Methods

3.1. Moving Principal Component Analysis (MPCA)

The purpose of the Principal Component Analysis (PCA) is to identify dependencies behind a multivariate stochastic observation in order to obtain a compact description. Consider a data set, X, as expressed in equation (2), consisting of N_m observations on N_v variables. The rows are N_v-dimensional vectors representing the measurements of the variables at a given instant, whereas the columns are N_m-dimensional vectors corresponding to the time history of each variable.

$$X = \begin{bmatrix} X_{1,1} & X_{1,2} & \cdots & X_{1,N_v} \\ X_{2,1} & X_{1,2} & \cdots & X_{2,N_v} \\ \cdots & \cdots & \cdots & \cdots \\ X_{N_m,1} & X_{N_m,2} & \cdots & X_{N_m,N_v} \end{bmatrix} \tag{2}$$

The goal of PCA is to reduce the dimensionality of the data matrix by finding N_r new variables, where N_r is less than N_v. Termed principal components, these N_r new variables together account for as much of the variance in the original N_v variables as possible while remaining mutually uncorrelated and orthogonal. Each principal component is a linear combination of the original variables, and so it is often possible to ascribe meaning to what the components represent. The first component corresponds to the direction in which the projected observations have the largest variance. The second component is then orthogonal to the first and again maximizes the variance of the data points projected on it. Continuing in this manner, it is possible to compute all the principal components [22]. Equation (3) expresses the matrix of the observations, $\left[X\right]$, as a linear combination of a set of N_v orthogonal vectors, $\left[u_j\right]$.

$$\left[X\right] = \sum_{j=1}^{N_v} \left[Z_j\right]\left[u_j\right]^T \tag{3}$$

$\left[Z_j\right]$ is a vector containing the component scores of the j^{th} variable and $\left[u_j\right]$ is the j^{th} orthogonal vector. The component scores correspond to the coordinates of the original data in the new coordinate system defined by the orthogonal vectors, which are the eigenvectors computed from the covariance matrix $(N_v \times N_v)$ of the data set. As the first eigenvalues

represent the most important terms, it is possible to choose only the first N_r eigenvectors so that the final data set can be rewritten without significant loss of information, as expressed in equation (4):

$$[X] \cong \sum_{j=1}^{N_r} [Z_j][u_j]^T \tag{4}$$

In the Structural Health Monitoring field, PCA may be used for three primary purposes: i) evaluation of patterns in the data; ii) data cleansing; iii) data compression [23].

In the context of this work, it is used to enhance the discrimination between features of undamaged and damaged structures. The analysis of the behaviour in terms of eigenvalues and eigenfunctions of the covariance matrix of the data set gives a good indication of the damage initiation and provides information about the severity of the damage [13]. However, as the observation period increases, and therefore, the number of measurements becomes high, the time to detect the structural change also increases. When damage occurs, the influence of measurements in the undamaged state is much higher than that of the new measurements, leading to an increase in the time required for the eigenvector values to change enough in order to indicate damage.

To overcome this shortcoming, Posenato et al. [24] proposed Moving Principal Component Analysis (MPCA) that computes the principal components inside a moving window of constant size, containing N_w measurements $\left(N_w < N_m\right)$. For the k^{th} observation, the matrix X of the measurements becomes the following:

$$X(k) = \begin{bmatrix} X_{k-N_w+1,1} & X_{k-N_w+1,2} & \cdots & X_{k-N_w+1,N_v} \\ X_{k-N_w+2,1} & X_{k-N_w+2,2} & \cdots & X_{k-N_w+2,N_v} \\ \cdots & \cdots & \cdots & \cdots \\ X_{k,1} & X_{k,2} & \cdots & X_{k,N_v} \end{bmatrix} \tag{5}$$

Then, monitoring is carried out by observing the evolution of the principal components – the eigenvectors that are related to the first few eigenvalues. Damage is identified when there is a change in the values of the principal components. Considering that each $[Z_j]$ describes a major trend of the original data and that each component $u_{i,j}$ of the vector $[u_j]$ describes the influence of $[Z_j]$ for the i^{th} sensor, MPCA can be applied for anomaly detection in the

continuous static monitoring of civil structures. If the group of sensors considered in the analysis are correlated and if the structure has not been damaged, then the main eigenvalues remain stable with time. When something occurs on or in the structure, the signal from some sensors may vary with respect to others. As a consequence, the eigenvector components $u_{i,j}$ of the sensors closest to the zone involved by the new situation should highlight the variation. This feature enables damage identification as well as damage localization [13] [24].

Application of MPCA for damage detection using continuous monitoring data involves two phases: training and monitoring. In the training phase, the structure is assumed to behave in an undamaged condition. The aim of this initialization period is to estimate the variability of the time series and to define the thresholds for detecting anomalous behaviour in the monitoring phase. To do this, each eigenvector u_j at every time step during the reference period is stored and values, in each coordinate, $u_{i,j}$, for mean, $\mu_{i,j}$, and standard deviation, $\sigma_{i,j}$, are determined in order to define the corresponding thresholds. In the monitoring phase, the window continues moving along time series to compute new eigenvalues and eigenvectors at each time step. If there is no anomaly, the eigenvectors remain within these thresholds. When damage occurs, the components of covariance matrix change and as a consequence, so do values of eigenvalues. If the value of the c^{th} coordinate of the eigenvector u_j ($u_{c,j}$) exceeds the threshold bounds, an anomaly is flagged by sensor c at time k [25].

A key issue of MPCA is the dimension of the window, N_w. The value N_w should be sufficiently large so that it is not influenced by measurement noise and small enough to allow fast anomaly detection. Additionally, if the time series has periodic variability, the window size should be a multiple of the period, so that mean values are stationary and eigenvalues of the covariance matrix do not have periodic behaviour [26].

Comparing MPCA with PCA, the use of a moving window rather than all measurements has three main advantages. First, the calculation of process parameters is faster. Second, detection of anomalous behaviour is more timely because the old measurements do not bias the results. Finally, once new behaviour is identified, the definition of a new training phase corresponding to the new state of the structure allows detection of further anomalies [24].

3.2. Robust Regression Analysis (RRA)

Many problems in engineering and science involve exploring the relationships between two or more variables. Regression analysis is a statistical technique that is very useful for these types of problems [27]. It is normally used to detect anomalous behaviour in two ways. One method consists in evaluating how the distance between the points and the regression line change with time. The other consists of observing the evolution of the coefficients of the regression. Anomalies are identified whenever a significant variation is observed [26].

The algorithm involves the calculation of a robust regression line between two sensors for the reference period which is used to discover anomalies in the trends of the measurements. The linear relation between two variables, X_i and X_j, can be written as:

$$\hat{X}_j = aX_i + b \tag{6}$$

Where $\hat{X}_j$ represents the value of X_j calculated according to the linear relation and a and b are the coefficients of the robust regression line estimated from measurements in the training phase. The method used to compute the coefficients in equation (6) involves assigning a weight to each data point. Weighting is done automatically and iteratively using a process called *iteratively reweighted least squares*. In the first iteration, each point is assigned equal weight and model coefficients are estimated using ordinary least squares. At subsequent iterations, weights are recomputed so that points farther from model predictions in the previous iteration are given lower weight. Model coefficients are then recomputed using weighted least squares. The process continues until the values of the coefficient estimates converge within a specified tolerance [28]. An advantage of robust regression in comparison with traditional regression is its insensitivity to outliers.

In this work damage detection is based on the first approach presented above, which involves the calculation of $\hat{X}_j$ at every instant of observation and the corresponding differences $\left|X_j - \hat{X}_j\right|$. As in the MPCA, application of RRA for anomaly detection during continuous monitoring includes two phases: training and monitoring. In the training phase the structure is assumed to behave normally (no damage). During the reference period, the mean, μ_j, and the standard deviation, σ_j, of the differences $\left|X_j - \hat{X}_j\right|$ are determined in order

to define the corresponding thresholds. In the monitoring phase, at each time step k, the differences $\left|X_j - \hat{X}_j\right|$ within a window ranging from time step $k - N_{test}$ to k, in which N_{test} is the window size, are evaluated. If N_{out} measurements, in which $N_{out} \leq N_{test}$, are out of the threshold bounds, the anomaly is detected by the variable pairs X_i and X_j.

In addition to the advantage of being insensitive to outliers and missing data, RRA is capable of adapting to the new state of a structure for identifying further anomalies by redefining a new training phase after an anomaly is identified.

4. Application to numerically simulated data

4.1. Simulated Data

The proposed approach will be tested on data obtained through using the numerical model presented in Section 2.1. A load variability of ±10% around a service load of 8.75 kN and uniformly distributed noise in the measurements as described in Section 2.1 will be assumed. Consider a period of observation in which the response of 1500 crossings of the structure was collected. The first 1000 crossings are the baseline condition (undamaged) and the latest 500 are the damaged condition. As described above, the damage scenario under consideration consists of a 20% reduction in the stiffness of a 30 cm length beam element (see Fig. 1).

According to the two types of time series that can be built using the moving-load data presented above, the following two types of analysis are performed:

i) 4 time histories of type I (4 transducers employed);

ii) 44 time histories of type II (11 load positions, as depicted in Fig. 1, times 4 transducers).

Fig. 6 and Fig. 7 present respectively, a time series of type I and type II, for the rotation over the left support (RLB). The former involves the whole influence line whereas the latter is for load position 3, which is the damage location (see Fig. 1). Fig. 6.b and Fig. 7.b are magnifications of parts of Fig. 6.a and Fig. 7.a respectively, considering 23 crossings before and after the occurrence of damage. No significant differences in the signals, indicating the occurrence of damage, can be observed. Although in Fig. 7 there is a slight difference between the response before and after damage, a small increase in the load variability would hide this difference and, thus, the occurrence of damage might not be detected. Therefore, the application of more sophisticated data processing is necessary.

In this section, using these two types of time series, two data-driven methods – Moving Principal Component Analysis (MPCA) and Robust Regression Analysis (RRA) – will be applied to detect both the occurrence and the location of damage. The capability of each method, as well as the time to detection will be evaluated. Throughout this paper the time to detection, also referred to as *delay*, corresponds to the number of crossings observed between the occurrence and the detection of the damage.

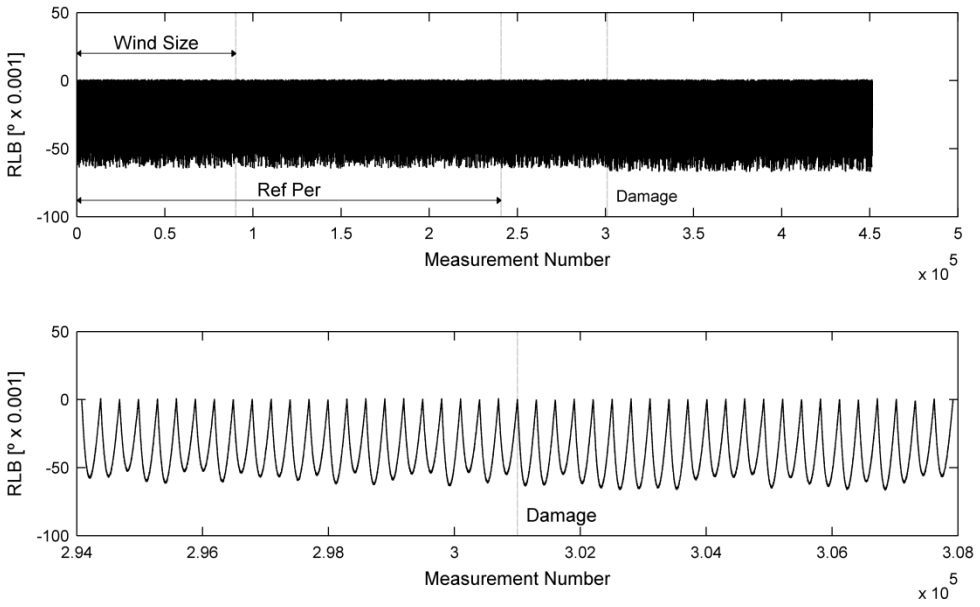

Fig. 6 – Time-series type I, of the rotation over the left support (RLB): a:) Whole period; b) Expansion of part of the whole period.

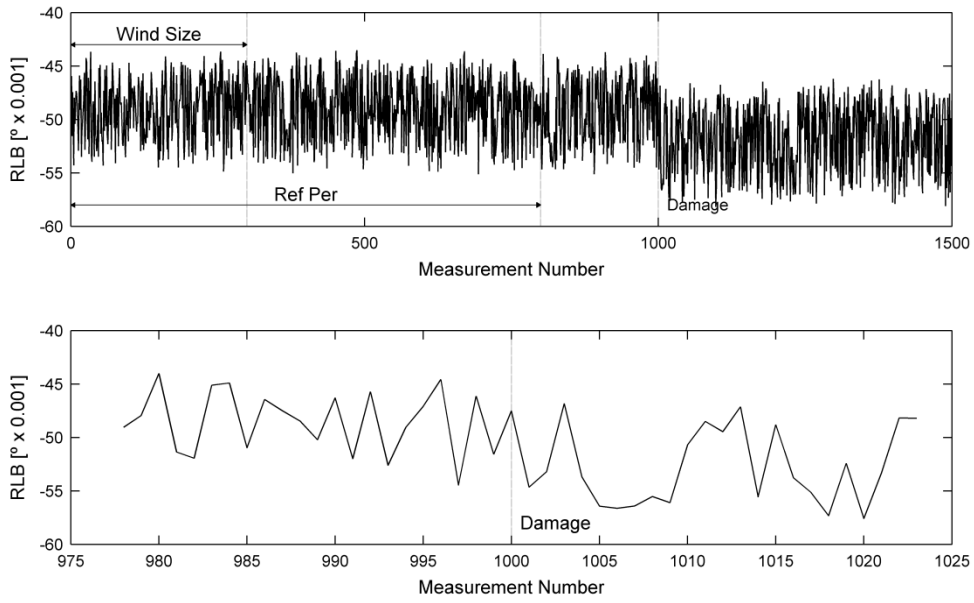

Fig. 7 – Time-series type II, of the rotation over the left support (RLB) for load position 3:. a) Whole period; b) Expansion of part of the whole period.

4.2. Moving Principal Component Analysis (MPCA)

MPCA was applied to both data sets – type I and type II. To compare the performance of the method the parameters such as reference period, window size and thresholds, were assumed to have the same values for both types of analysis.

As mentioned above, application of MPCA to Structural Health Monitoring involves an initial phase where the structure is assumed to behave normally and this is called the training phase. The aim of this reference period is to estimate the variability of the time series and to define thresholds for detecting anomalous behaviour. In this study, the training phase comprised 800 crossings, in which both the mean, μ_j, and the standard deviation, σ_j, were computed in order to define thresholds for damage detection.

During the monitoring phase, as soon as q consecutive points exceed the threshold a structural change is flagged. The requirement of q consecutive points exceeding the thresholds in order to flag a structural change increases the reliability of the methodology by preventing false positive indications of damage. In this work, the thresholds were assumed to be $\mu \pm 9\sigma$ and $q = 10$. These unusually high levels are necessary to avoid false positives arising from the response of a beam subjected to moving loads. The window size, N_w, was defined by taking into account the features of the time series.

The time-series type I presents periodic variability (Fig. 6), corresponding to the number of positions observed in each crossing ($m = 301$). Therefore, it should be a multiple of m. In addition, the time series type II does not present periodic variability (Fig. 7) given that each time series contains the response at a given position for the successive crossings. Therefore, the variability is due to both the measurement noise and the variability in the load. Thus, a window comprising 300 crossings, a multiple of the period in time series of type I, is used and this size means that calculations are not significantly influenced by measurement noise in time-series type II. The Window Size (Wind Size) and the Reference Period (Ref Per) are marked both in Fig. 6 and Fig. 7.

The application of MPCA requires computing the principal components (PC) inside a moving window of constant size along the time series. In practice computing PC of a data set S entails [29]:

i. subtracting off the mean of each measurement type, as expressed in equation (7) – denoted as normalization *a* – where S_i represents the time series of the variable *i* (which may be the time history of a given sensor in the data set of type I or the time history of a given sensor for a given load position in the data set of type II) and μ_i is the corresponding mean;

$$X_i = S_i - \mu_i \tag{7}$$

ii. computing the eigenvectors of the covariance matrix Σ of the data set.

As previously described, when something occurs on or in the structure, measurement data from some sensors may vary with respect to data from other sensors. As a consequence, the main eigenvalues change and the eigenvector components $u_{i,j}$ of the sensors closest to the zone involved by the new situation should highlight a variation. If the value of the c^{th} coordinate of the eigenvector u_j ($u_{c,j}$) exceeds the threshold bounds, an anomaly is flagged by sensor c at time k and, thus, it is expected that damage is located close to sensor c. The figures presented below illustrate the results of the MPCA. They show the evolution of the coordinate of the first principal component (eigenvector) that first exceeds the thresholds, i.e., the coordinate that first flags the damage. As the sensors closest to the damage should highlight the variation, it is expected that the sensor related to this coordinate may be near the damage. In particular, for time series type II, as each time series is related to a load position, it may be seen as a time series of a sensor. Therefore, it is expected that damage may be localized by the time series related to LP3, placed over the damage, or LP2 or LP4, close to the damage.

Fig. 8 presents the time series of the first component for the RLB of the first principal component given by MPCA using the time series of type I. Fig. 9 presents the time history of the first component for the HDR and load position 3 using the time series of type II. As can be seen in the figures, the data processing using MPCA allows the early detection of changes in the structural response and the location of damage. Using the time-series type I, the damage was detected 15 crossings after the occurrence of the damage (Fig. 8). Using the time-series type II, the first coordinate of the first principal component exceeding the thresholds (Fig. 9) corresponds to load position 3, which matches the location of the stiffness reduction (see Fig. 1). In this case, the delay was 27 crossings.

However, as it will be shown, after performing several analysis adopting different random sequences, in terms of load variability and noise in the measurements, it was observed that the damage location is seldom correctly identified.

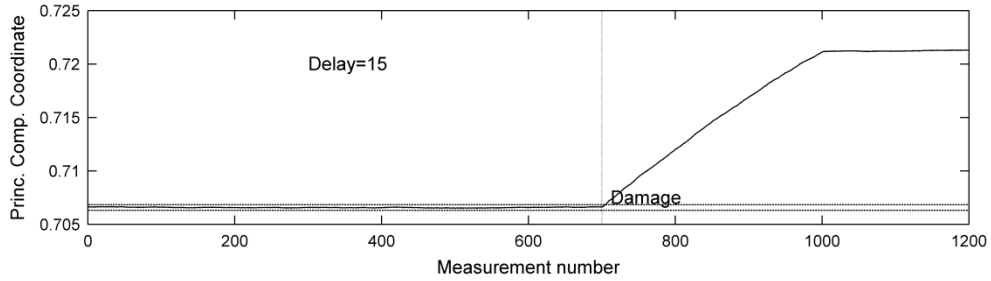

Fig. 8 – Time history of the coordinate corresponding to the RLB of the first principal component applying MPCA on time-series type I using normalization a.

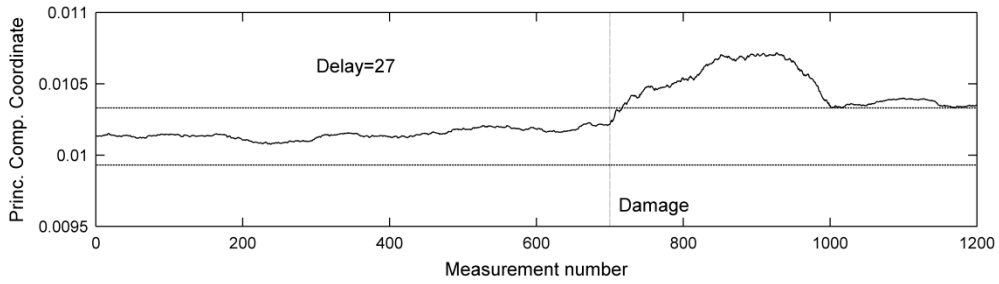

Fig. 9 – Time history of the coordinate corresponding to the HDR for load position 3 of the first principal component applying MPCA on time-series type II using normalization a.

Consider an additional step prior to the calculation of the eigenvectors. After subtracting the mean of each measurement type, the data is divided by the standard deviation of each variable, σ_i, as expressed in equation (8). This procedure will be denoted as normalization *b*.

$$X_i = \frac{S_i - \mu_i}{\sigma_i} \tag{8}$$

The results presented in Fig. 10 and Fig. 11 refer to the MPCA using pre-processed data through the normalization *b*. Fig. 10 presents the time history of the coordinate corresponding to RRB of the first principal component using the time-series type I. The time history of the coordinate corresponding to RLB at load position 3 of the first principal component using the time-series type II is depicted in Fig. 11. As in the normalization *a* procedure, the results adopting the normalization *b* procedure show that the occurrence and the location of the damage may be detected. Again, the coordinate of the principal component that first exceeds the threshold corresponds to the load position 3. The delay using time series of type I and II was, respectively, 79 and 32 crossings.

As previously noted, damage is detected when a principal component coordinate value exceeds the threshold bounds. Afterwards, as soon as the moving window contains data of the damaged condition only, a new state of the structure is defined. In Fig. 8 and Fig. 10, as after damage the value of the coordinate stabilizes in a different value than that before damage, the modification into a new state is clear. In Fig. 9, in spite of being very close, the new state is different from the old one. However, in Fig. 11 the two states are similar. This is due to the type of data and normalization used. As the data is divided by the standard deviation, the normalized data of the new state happens to be similar to that of the old state. The same does not happen in Fig. 10 because it includes all the influence lines and as their shape change due to damage, the new state is different from the old one, even after normalization b.

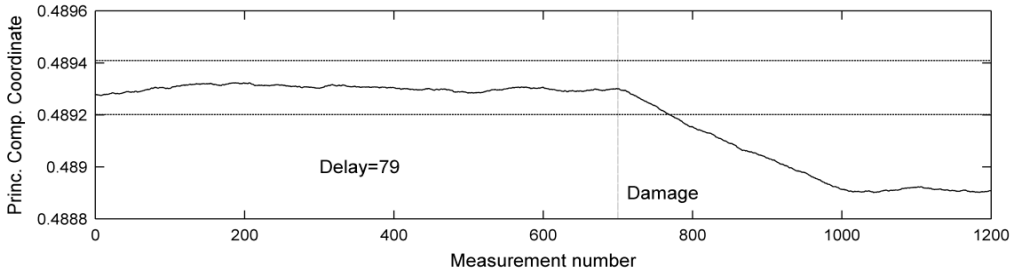

Fig. 10 – Time history of the coordinate corresponding to the RRB of the first principal component applying MPCA on time-series type I using normalization b.

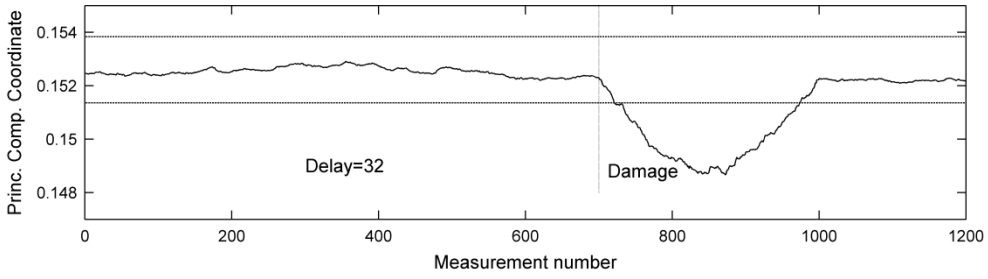

Fig. 11 – Time history of the coordinate corresponding to the RLB for load position 3 of the first principal component applying MPCA on time-series type II using normalization b.

Comparing Fig. 8 with Fig. 10, it is observed that the time to detect the damage occurrence is much more pronounced in the latter than in the former. Furthermore, in Fig. 8 the variation in the component is much clearer. Therefore, the normalization *a* is more suitable than normalization *b* to detect the occurrence of damage using time-series type I. Comparing Fig. 9 with Fig. 11 one observes the opposite. Although in this case the time to detect the occurrence of damage using the normalization *a* is smaller, as it will be shown, the normalization *b* leads to lower time to detection and to more reliable results regarding the localization of damage.

In order to validate the conclusions drawn above, 100 analyses adopting different random sequences, in terms of load variability and noise in the measurements, were performed. The study involved the two types of data sets – type I and II – and the two normalization procedures – *a* and *b*. The results are summarized in the tables 1 to 3.

Using time-series type I, there is no false-positive indication of damage in either normalization procedures. This means that the occurrence of damage is correctly identified in every case. Table 1 presents the comparison in terms of time to detection, given by MPCA applied to the time-series type I, between both normalization procedures. It is observed that the normalization procedure *a* provides the best results regarding the time to detection of damage. The time to detection using the normalization *a* is significantly smaller than that using normalization *b*.

The comparison in terms of damage location, given by MPCA applied to the time-series type II, between both normalization procedures is shown in Table 2. The false-positive indication of damage is similar in each normalization procedure – 2% and 3% in normalization procedures *a* and *b*, respectively. However, concerning the identification of the damage location, the results obtained using the normalization procedure *b* are significantly better. The damage location is correctly identified – LP3 – in more than 70% of the cases. Furthermore, considering that the identification of contiguous load positions (LP2 and LP4) is also acceptable regarding the location of damage (see Fig. 1), only in 15% of the cases the damage location is not correctly identified. On the other hand, using the normalization procedure *a* the location of damage is incorrectly identified in almost 40% of the cases.

Table 3 presents the comparison in terms of time to detection, given by MPCA applied to the time-series type II, between both normalization procedures. The data presented in the table includes the true-positive damage detection cases associated with load positions 2, 3 and 4 only. The time to detection using the normalization procedure *b* is smaller. Therefore, the normalization procedure *b* applied before the MPCA on the data set of type II provides the most reliable results in terms of damage location and lower times to detection.

Table 1 – Time to detection using time-series type I.

Normalization	a	b
Minimum	13	25
Maximum	28	157
Mean	18.4	58.6
Standard deviation	3.2	23.9

Table 2 – Damage location (load position that signalizes the occurrence of damage) using time-series type II.

Normalization	a	b
False-positives	2	3
Load position 3	31	72
Load positions 2 and 4	31	13
Other load positions	36	12

Table 3 – Time to detection using time-series type II.

Normalization	a	b
Minimum	13	16
Maximum	92	63
Mean	41.2	31.3
Standard deviation	16.9	9.5

4.3. Robust Regression Analysis (RRA)

The procedure adopted to detect damage using RRA involves determining whether there are points lying far from the regression line estimated during a reference period. This requires calculation of $\hat{X}_j$ and the differences $\left|X_j - \hat{X}_j\right|$, denoted as residuals, during the training and monitoring phases. As in the MPCA, the training phase involved 800 crossings, in which the mean, μ_j, and the standard deviation, σ_j, were computed in order to define thresholds for damage detection. During the monitoring phase, as soon as at least 9 points (N_{out}) out of 10 consecutive points (N_{test}) exceeded the threshold, assumed to be $\mu \pm 3\sigma$, a structural change is flagged. The procedure of flagging damage only when at least N_{out} points, out of N_{test} consecutive points, exceed the threshold bounds improves the reliability of the method, preventing false positive indications.

In statistics the correlation coefficient is a measure of the correlation (linear dependence) between two variables X and Y. It is widely used as a measure of the strength of linear dependence between two variables. Consider a data set of type I containing one crossing only,

with noise in the measurements as described in Section 2.1. Table 4 presents the correlation coefficients for the influence lines of the four sensors.

Table 4 – Correlation coefficients between the sensors (1 crossing).

	VDM	HDR	RLB	RRB
VDM	1	0.997	0.953	-0.954
HDR	0.997	1	0.956	-0.957
RLB	0.953	0.956	1	-0.832
RRB	-0.954	-0.957	-0.832	1

Although values for the correlation coefficients for all sensor pairs are relatively high (higher than 0.8), the relation between the sensors response is not linear. Fig. 12 presents the relation between the vertical displacement at mid-span (VDM) and the horizontal displacement at the roller support (HDR) during one crossing. Fig. 12 a) presents both the relation between the measurements and the corresponding regression line whereas Fig. 12 b) presents the residuals between the measurements and the predictions computed with the regression line. Although the correlation coefficient is very close to 1 ($\rho = 0,997$), it is clear that the relationship between responses VDM and HDR is not linear, see Fig. 12 b).

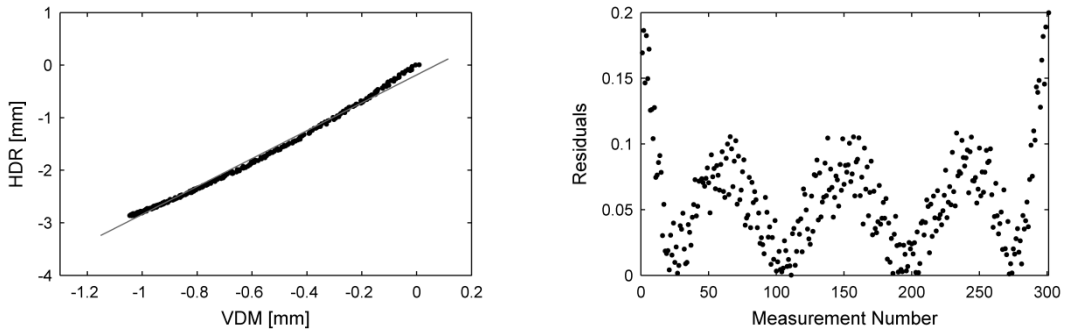

a) Values b) Residuals

Fig. 12 – Relationship between VDM and the HDR.

Fig. 13 presents the relationship between the vertical displacement at mid-span (VDM) and the rotation over the left support bearing (RLB) during one crossing. Fig. 13 a) presents both the relationship between the measurements and the corresponding regression line whereas Fig. 13 b) presents the residuals between the measurements and the predictions computed with the regression line. In both figures it is clear that the relationship between these responses (VDM and RLB) is not linear. Therefore it may not be appropriate to apply the RRA using time-series type I.

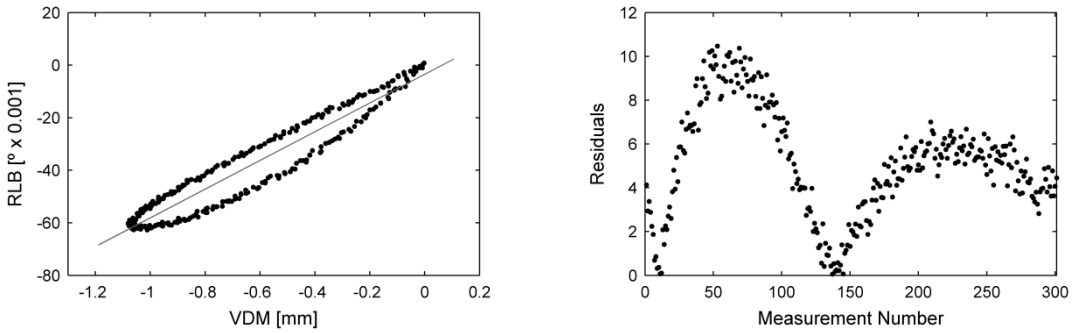

a) Values b) Residuals

Fig. 13 – Relationship between VDM and the RLB.

Consider a dataset of time-series type II, 100 crossings, in the baseline condition, with load variability of ±10% around a service load of 8.75 kN and noise in the measurements as described in Section 2.1. Fig. 14 presents the relationship between the vertical displacement at mid-span (VDM) and the horizontal displacement at the roller support (HDR) when the load is, in both cases, at mid-span, LP6 (see Fig. 1). Fig. 14 a) presents both the relationship between the measurements and the regression line whereas Fig. 14 b) presents the residuals of taking the difference between measurements and the predictions computed with the regression line. The relationship between these responses is linear.

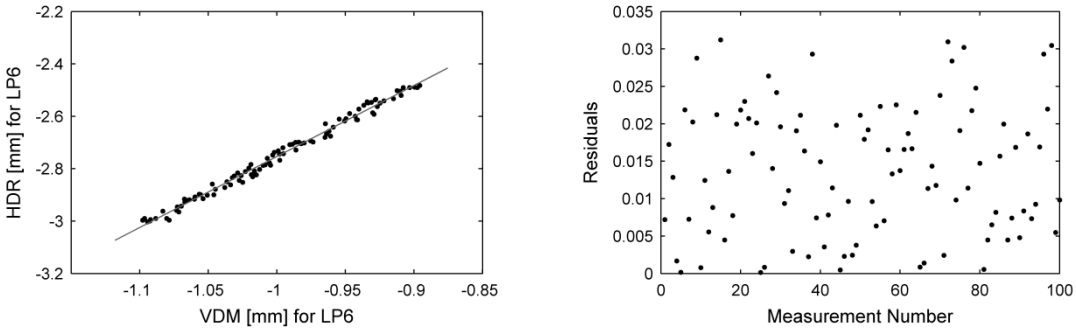

a) Values b) Residuals

Fig. 14 – Relationship between the VDM and HDR when the load is at mid-span, LP6.

Therefore the RRA will be applied using only the time-series type II. The results of the RRA applied on the data set of type II, containing 44 time histories, as described in Section 4.1, are presented below.

Fig. 15 presents the residuals of measurements and predictions computed with the regression line using RRA obtained with the time series corresponding to the HDR response for load position 2 and the VDM for load position 5 – one of the pairs that present the smallest time to

detection. The damage is detected 9 crossings after its occurrence. The plot shows a clear change in the structural condition.

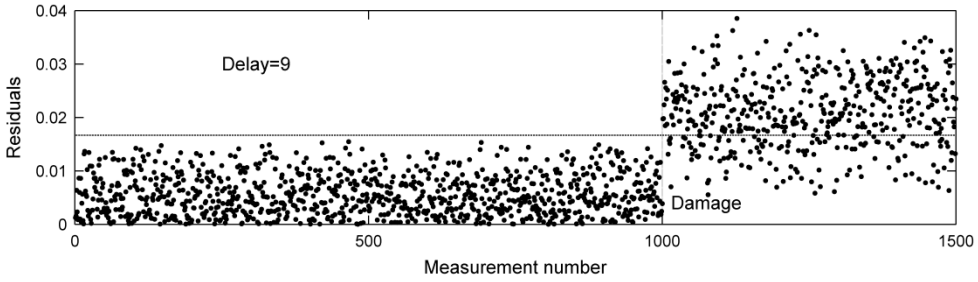

Fig. 15 – Residuals obtained applying RRA to the relation between the time-series type II of the HDR for load position 2 and the VDM for load position 5.

Fig. 16 presents the relationship between the responses recorded by the HDR for load position 2 and the VDM for load position 5 before (black) and after (gray) damage. The effect of the occurrence of damage is clearly flagged by the shift of the relationship between the responses before and after damage.

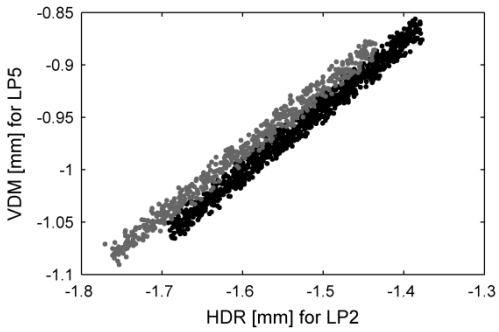

Fig. 16 – Relationship between the time-series type II of the HDR for load position 2 and the VDM for load position 5 before (black) and after (gray) damage.

In order to validate the applicability of the RRA as a reliable damage detection procedure, using time-series type II, 100 analysis adopting different random sequences, both in terms of load variability and noise in the measurements, were performed. In every case, the occurrence of damage was correctly identified. Moreover, the time to detection in every situation was nine crossings.

5. Conclusions

This paper discusses the application of data-driven methods on moving-load data in order to detect the occurrence as well as the location of damage. The present methodology takes into account the quasi-static structural response only and thus, the dynamic component is not included. Using a damage scenario of a local crack in a reinforced concrete element, simulated

as a stiffness reduction in a beam element, time series of moving-load data is useful input for behaviour-model-free (non-physics-based) methods. Based on the results described in this paper, the following conclusions are drawn:

i. Data processing using MPCA allows the early detection of changes in the structural response and the location of damage. Two types of normalization of the data prior to the calculation of the principal components were tested. Normalization *a* consists of subtracting the mean prior to the calculation of the covariance matrix. In normalization *b*, the data is also divided by the standard deviation. The results showed that: i) using time-series type I and normalization *a*, MPCA allows the earliest detection of damage; ii) using the time-series type II and normalization *b* locates damage the best.

ii. Applying RRA on time-series type I was not appropriate because the response relationships are not linear. Using time-series type II, the occurrence of damage was detected. However, the method does not provide information related to damage location.

iii. In general, the time to detection using RRA is smaller than MPCA. Therefore, the combination of both methods provides the most complete information on structural condition.

Acknowledgements

The first author acknowledges FCT - Portuguese Foundation for Science and Technology for the financial support to PhD Grant SFRH/BD/42315/2007. The authors thank I. Laory for his support related to the application of MPCA and RRA.

References

[1] L.A. Bisby, An Introduction to Structural Health Monitoring, ISIS Educational Module 5, ISIS Canada, 2004.

[2] Z. Lounis, Aging highway bridges, Canadian Consulting Engineer, 48 (2007) 30-34.

[3] L. Shoup, N. Donohue, M. Lang, The Fix We're in For: The State of Our Nation's Bridges, Transportation for America (T4 America), 2011.

[4] R. Kaschner, C. Cremona, D. Cullington, Review of current procedures for assessing load carrying capacity, Bidge Management in Europe (BRIME), 1999.

[5] G. Sedlaccek, O. Hechler, A. Losche, B. Kuhn, Guidelines for monitoring of steel railway bridges, Sustainable Bridges, 2007.

[6] J.M.W. Brownjohn, Structural health monitoring of civil infrastructure, Philos. Trans. R. Soc. A-Math. Phys. Eng. Sci., 365 (2007) 589-622.

[7] C.R. Farrar, K. Worden, An introduction to structural health monitoring, Philos. Trans. R. Soc. A-Math. Phys. Eng. Sci., 365 (2007) 303-315.

[8] Q. Zhang, Y. Zhou, Investigation of the applicability of current bridge health monitoring technology, Struct. Infrastruct. Eng., 3 (2007) 159-168.

[9] K. Worden, J.M. Dulieu-Barton, An overview of intelligent fault detection in systems and structures, Struct. Health Monit., 3 (2004) 85-98.

[10] ASCE SEI Comittee on Structural Identification of Constructed Systems, Structural Identification (St-Id) of Constructed Facilities - Approaches, Methods and Technologies for Effective Practice of St-Id, 2011.

[11] P. Moyo, J.M.W. Brownjohn, Detection of anomalous structural behaviour using wavelet analysis, Mech. Syst. Signal Proc., 16 (2002) 429-445.

[12] P. Omenzetter, J.M.W. Brownjohn, Application of time series analysis for bridge monitoring, Smart Mater. Struct., 15 (2006) 129-138.

[13] F. Lanata, A. Del Grosso, Damage detection and localization for continuous static monitoring of structures using a proper orthogonal decomposition of signals, Smart Mater. Struct., 15 (2006) 1811-1829.

[14] D. Posenato, P. Kripakaran, D. Inaudi, I.F.C. Smith, Methodologies for model-free data interpretation of civil engineering structures, Comput. Struct., 88 (2010) 467-482.

[15] A.J. Cardini, J.T. DeWolf, Long-term structural health monitoring of a multi-girder steel composite bridge using strain data, Struct. Health Monit., 8 (2009) 47-58.

[16] S. Chakraborty, J.T. DeWolf, Development and implementation of a continuous strain monitoring system on a multi-girder composite steel bridge, J. Bridge Eng., 11 (2006) 753-762.

[17] R. Zaurin, F.N. Catbas, Structural health monitoring using video stream, influence lines, and statistical analysis, Struct. Health Monit., 10 (2011) 309-332.

[18] I.-Y. Choi, J.S. Lee, E. Choi, H.-N. Cho, Development of elastic damage load theorem for damage detection in a statically determinate beam, Comput. Struct., 82 (2004) 2483-2492.

[19] S. Stohr, M. Link, R. Rohrmann, W. Rucker, Damage detection based on static measurements on bridge structures, in: IMAC XXIV - 24th Conference and Exposition on Structural Dynamics, St. Louis, Missouri, USA, 2006, CD format, 12 pages.

[20] A. González, E.J. OBrien, Calculation of the influence line of a bridge using a moving vehicle, in: IABMAS'08 - 4th International Conference on Bridge Maintenance, Safety and Management, H.-M. Koh, D.M. Frangopol (Eds.), Seoul, Korea, 2008, pp. 3191-3198.

[21] P. Paultre, J. Proulx, M. Talbot, Dynamic testing procedures for highway bridges using traffic loads, J. Struct. Eng.-ASCE, 121 (1995) 362-376.

[22] M. Hubert, P.J. Rousseeuw, K. Vanden Branden, ROBPCA: a new approach to robust principal component analysis, Technometrics, 47 (2005) 64-79.

[23] E. Figueiredo, G. Park, J. Figueiras, C. Farrar, K. Worden, Structural Health Monitoring Algorithm Comparisons Using Standard Data Sets, Los Alamos National Laboratory, 2009.

[24] D. Posenato, F. Lanata, D. Inaudi, I.F.C. Smith, Model-free data interpretation for continuous monitoring of complex structures, Advanced Engineering Informatics, 22 (2008) 135-144.

[25] I. Laory, T.N. Trinh, I.F.C. Smith, Evaluating two model-free data interpretation methods for measurements that are influenced by temperature, Adv. Eng. Inform., 25 (2011) 495-506.

[26] D. Posenato, Model-Free Data Interpretation for Continuous Monitoring of Complex Structures, Ph.D. Thesis, École Polytechnique Fédérale de Lausanne, 2009.

[27] D.C. Montgomery, G.C. Runger, Applied Statistics and Probability for Engineers, John Wiley, New York, 1999.

[28] MatLab, MATLAB R2012.a Statistics Toolbox: Robust Regression, The MathWorks.

[29] J. Shlens, A tutorial on principal component analysis, 2009, www.snl.salk.edu/~shlens/pca.pdf.

List of Tables

Table 1

Normalization	a	b
Minimum	13	25
Maximum	28	157
Mean	18.4	58.6
Standard deviation	3.2	23.9

Table 2

Normalization	a	b
False-positives	2	3
Load position 3	31	72
Load positions 2 and 4	31	13
Other load positions	36	12

Table 3

Normalization	a	b
Minimum	13	16
Maximum	92	63
Mean	41.2	31.3
Standard deviation	16.9	9.5

Table 4

	VDM	HDR	RLB	RRB
VDM	1	0.997	0.953	-0.954
HDR	0.997	1	0.956	-0.957
RLB	0.953	0.956	1	-0.832
RRB	-0.954	-0.957	-0.832	1

List of Figures

Fig.	Caption	Format	Width [mm]	Height [mm]	Resol [dpi]
1	Frame model.	pdf	120	80	1000
2	Comparison of the influence lines in the baseline condition (black) and in the damaged condition (gray), left, and the corresponding differences between the responses, right.	tiff	150	150	1000
3	Comparison of the influence lines in the: i) baseline condition, under the reference moving load – ML (black); ii) baseline condition, under 1.10xML (light gray); iii) damaged condition, under 1.07xML (gray), left, and the differences between the responses ii-i (light gray) and iii-i (gray), right.	tiff	150	150	1000
4	Time-series type I, of the vertical displacement at mid-span (VDM).	tiff	150	38	1000
5	Time-series type II, of the vertical displacement at mid-span (VDM) when the load is at mid-span, LP6.	tiff	150	38	1000
6	Time-series type I, of the rotation over the left support (RLB):	-	-	-	-
6.a	Whole period;	tiff	150	38	1000
6.b	Expansion of part of the whole period.	tiff	150	38	1000
7	Time-series type II, of the rotation over the left support (RLB) for load position 3.	-	-	-	-
7.a	Whole period;	tiff	150	38	1000
7.b	Expansion of part of the whole period.	tiff	150	38	1000
8	Time history of the coordinate corresponding to the RLB of the first principal component applying MPCA on time-series type I using normalization a.	tiff	150	38	1000
9	Time history of the coordinate corresponding to the HDR for load position 3 of the first principal component applying MPCA on time-series type II using normalization a.	tiff	150	38	1000
10	Time history of the coordinate corresponding to the RRB of the first principal component applying MPCA on time-series type I using normalization b.	tiff	150	38	1000
11	Time history of the coordinate corresponding to the RLB for load position 3 of the first principal component applying MPCA on time-series type II using normalization b.	tiff	150	38	1000
12	Relationship between the VDM and the HDR.	-	-	-	-
12.a	Values	tiff	70	45	1000
12.b	Residuals	tiff	70	45	1000
13	Relationship between the VDM and the RLB.	-	-	-	-
13.a	Values	tiff	70	45	1000
13.b	Residuals	tiff	70	45	1000
14	Relationship between the VDM and HDR when the load is at mid-span, LP6.	-	-	-	-
14.a	Values	tiff	70	45	1000
14.b	Residuals	tiff	70	45	1000
15	Residuals obtained applying RRA to the relation between the time-series type II of the HDR for load position 2 and the VDM for load position 5.	tiff	150	38	1000
16	Relationship between the time-series type II of the HDR for load position 2 and the VDM for load position 5 before (black) and after (gray) damage.	tiff	70	45	1000

Figure 1

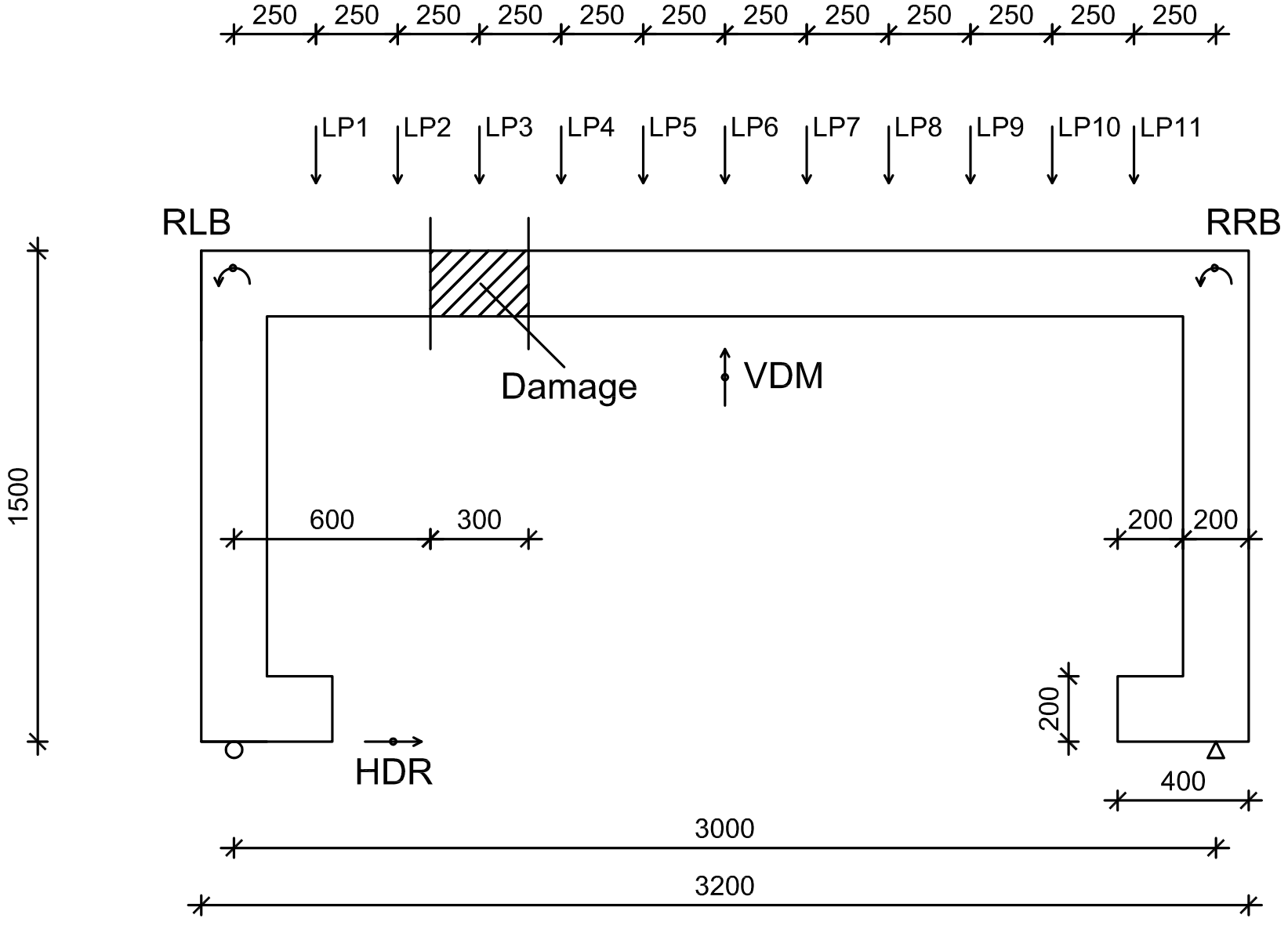
250 250 250 250 250 250 250 250 250 250 250 250
LP1 LP2 LP3 LP4 LP5 LP6 LP7 LP8 LP9 LP10 LP11
RLB
RRB
Damage
VDM
1500
600
300
200
200
200
HDR
400
3000
3200

Figure 2

Click here to download high resolution image

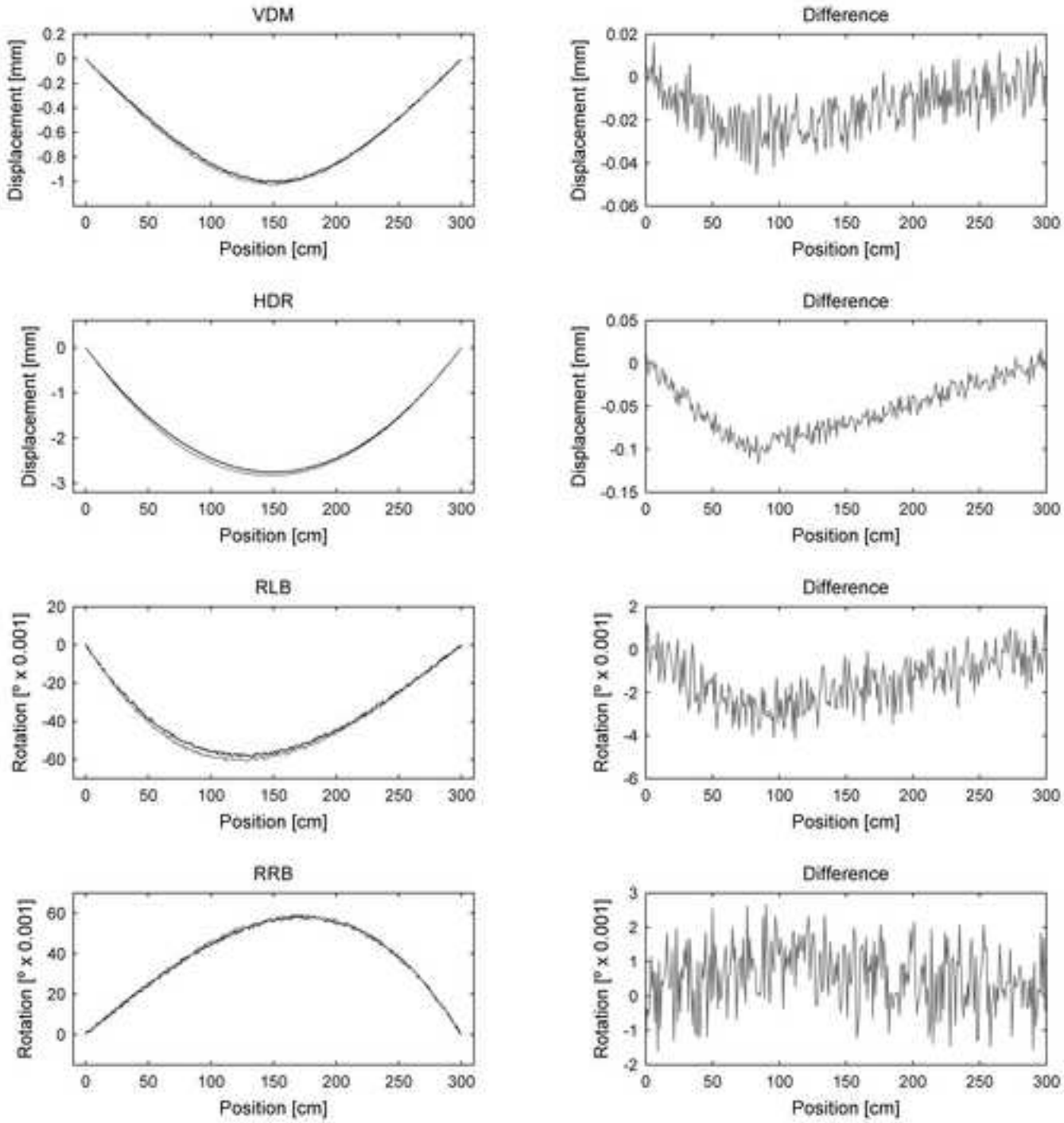

Figure 3

Click here to download high resolution image

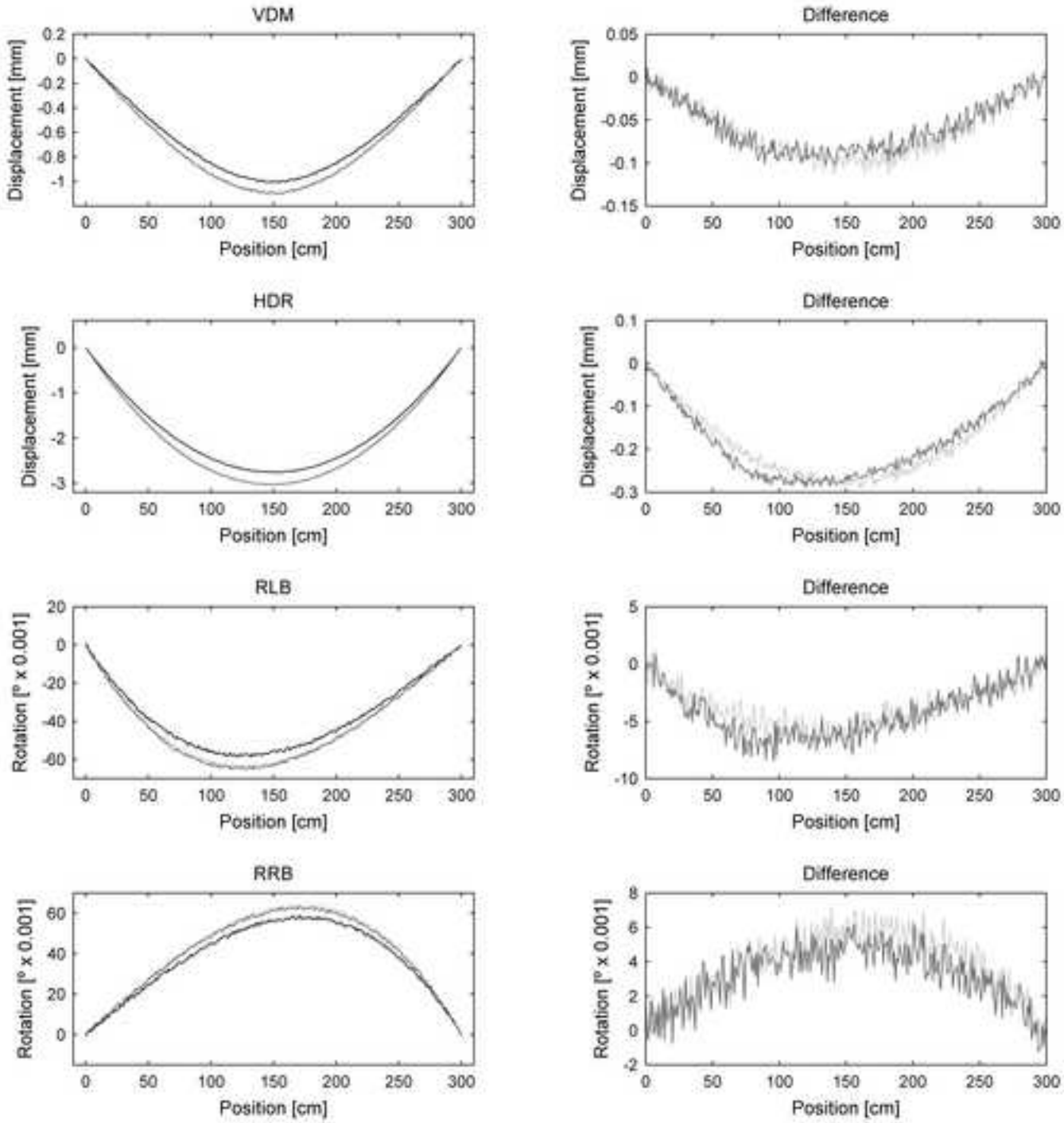

Figure 4

Click here to download high resolution image

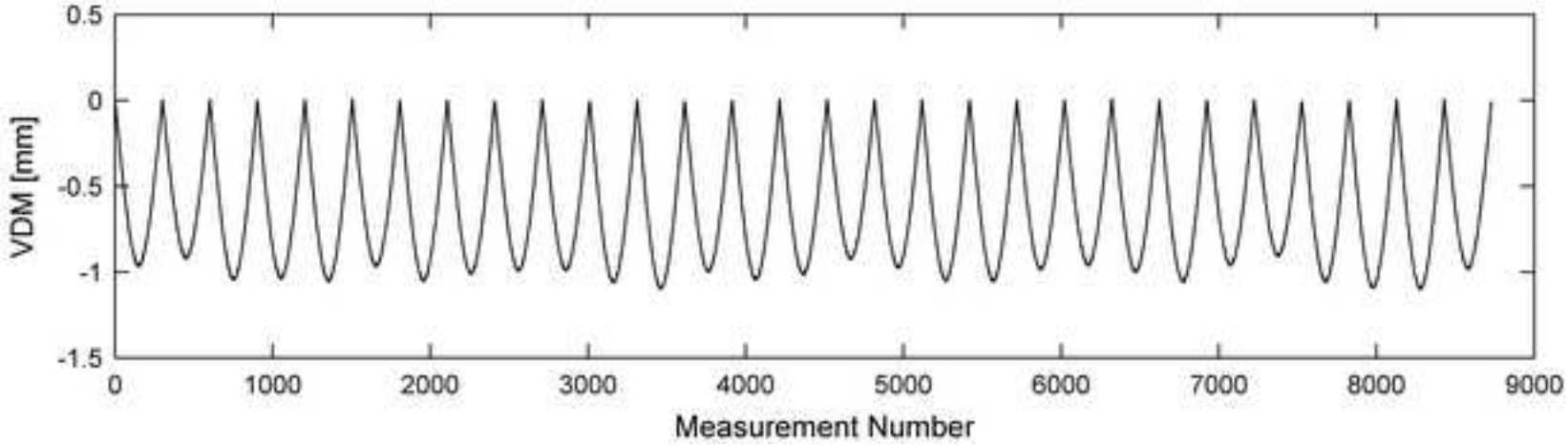

Figure 5

Click here to download high resolution image

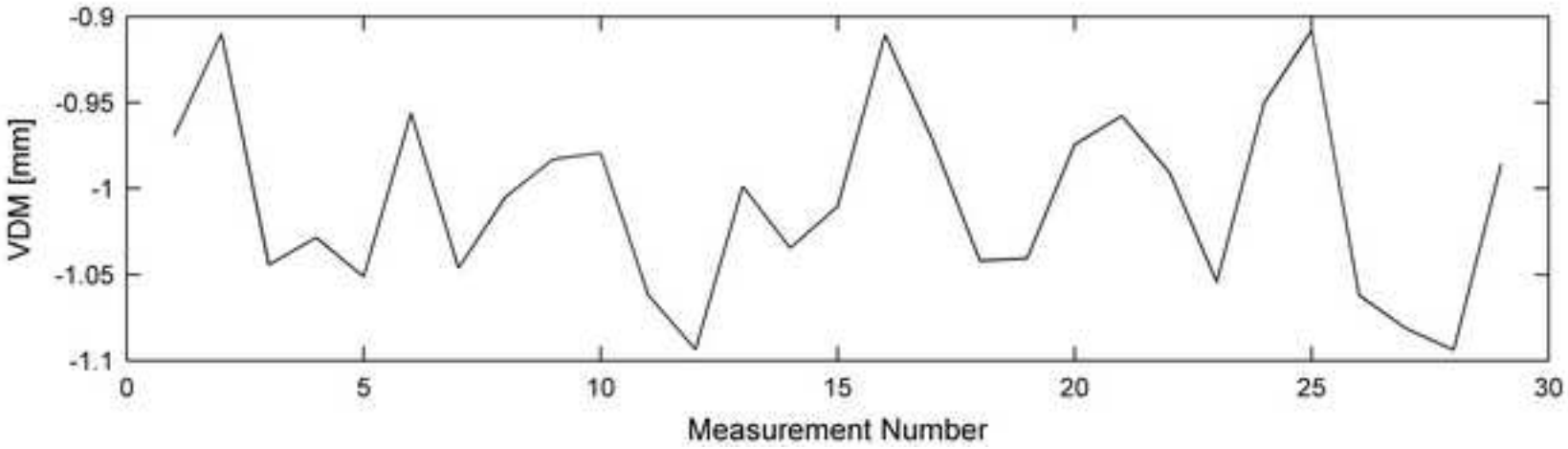

Figure 6.a
Click here to download high resolution image

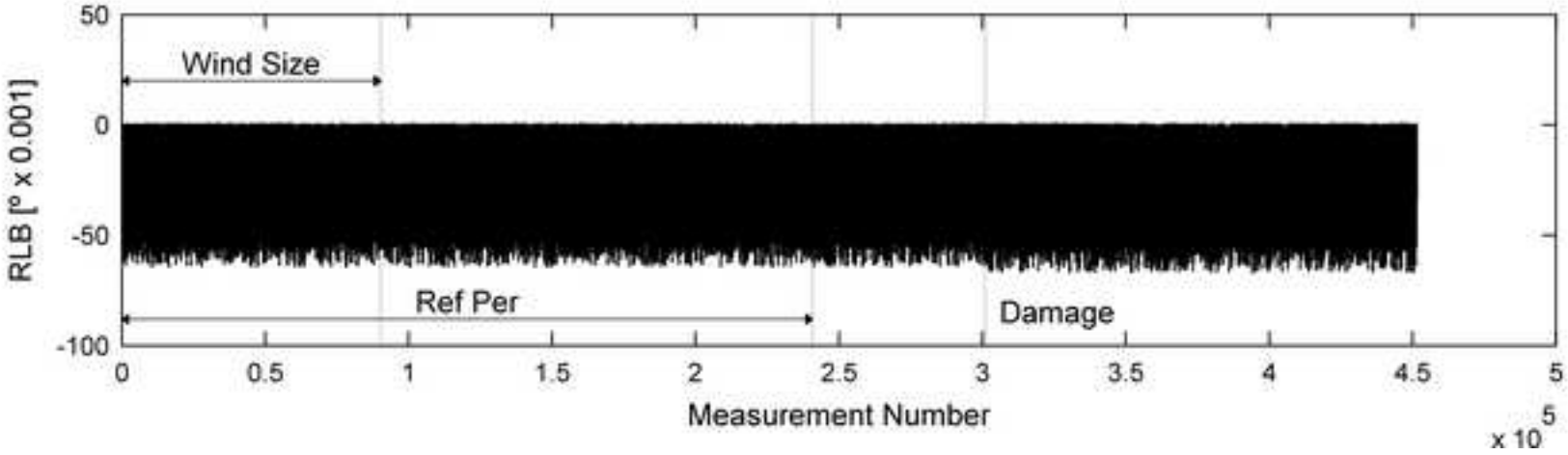

Figure 6.b

Click here to download high resolution image

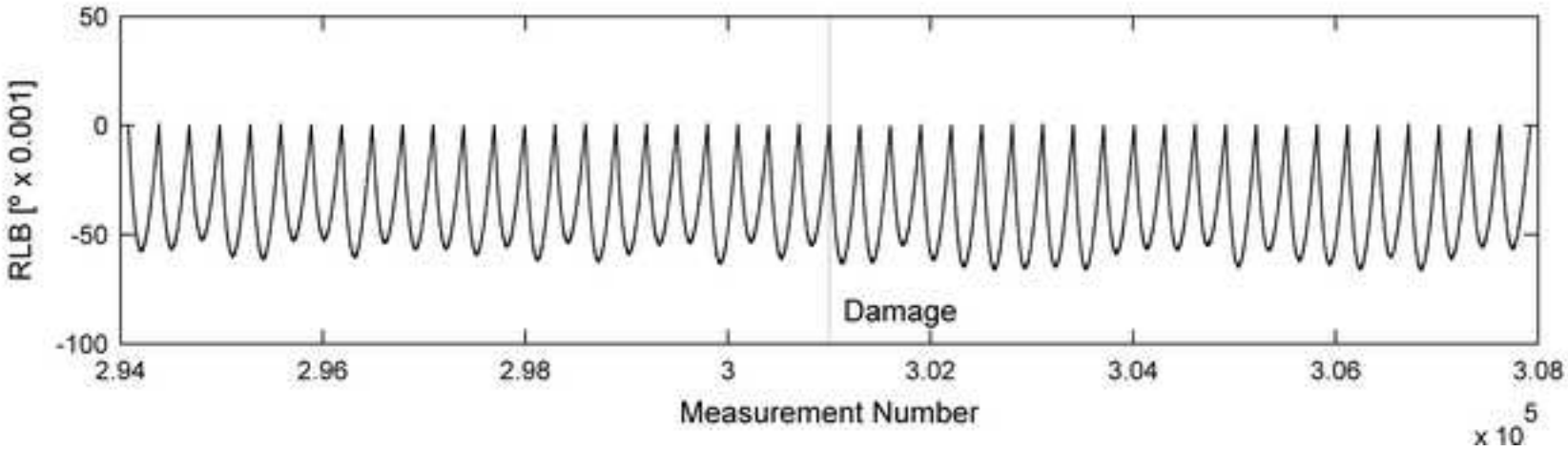

Figure 7.a

Click here to download high resolution image

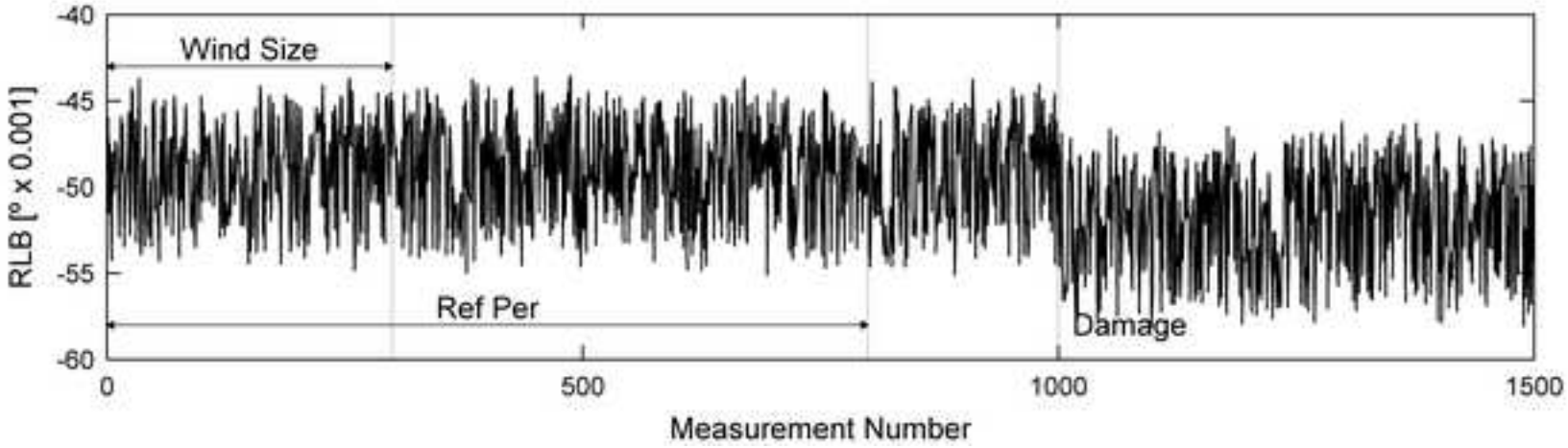

Figure 7.b

Click here to download high resolution image

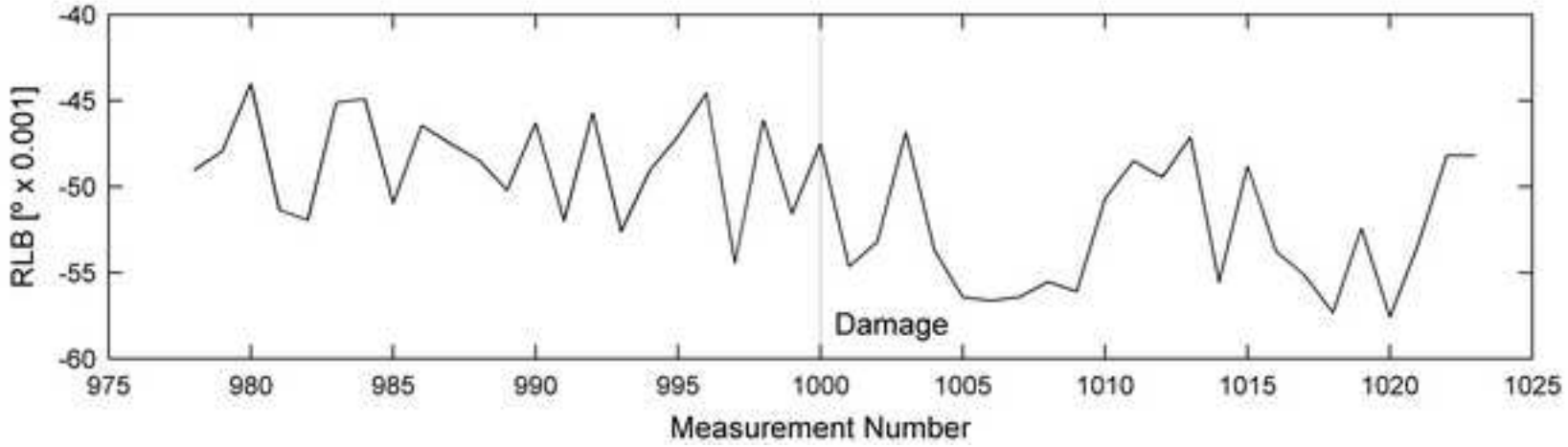

Figure 8

Click here to download high resolution image

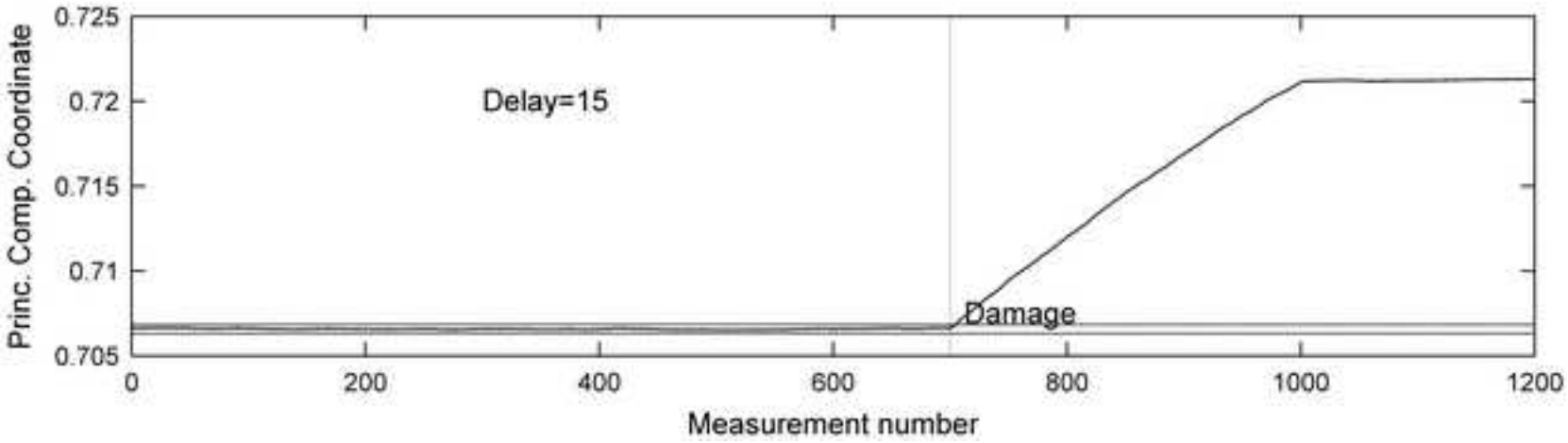

Figure 9

Click here to download high resolution image

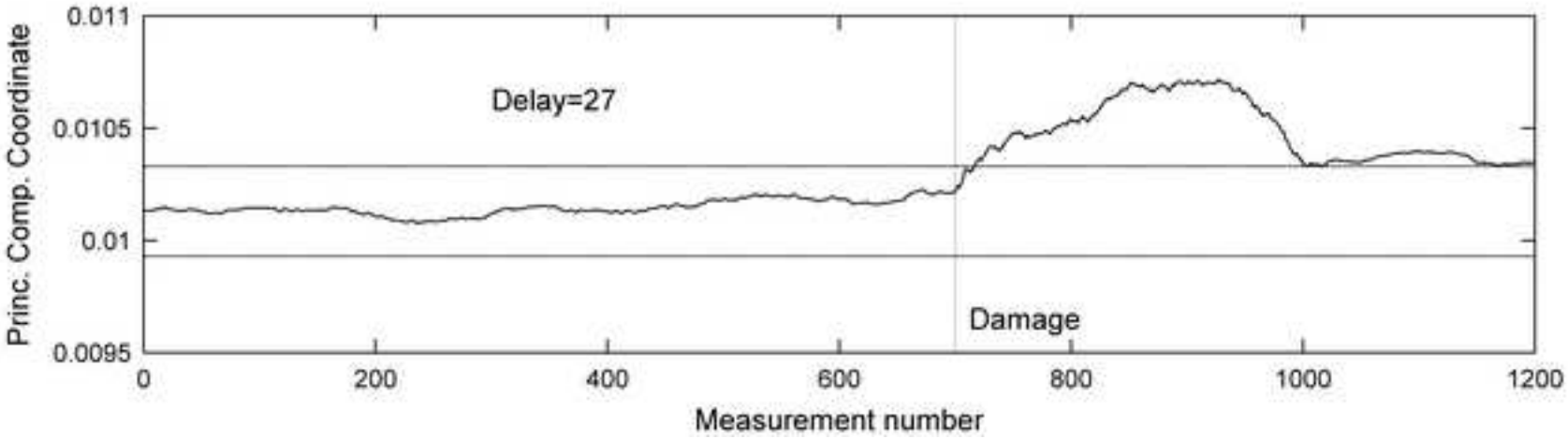

Figure 10

Click here to download high resolution image

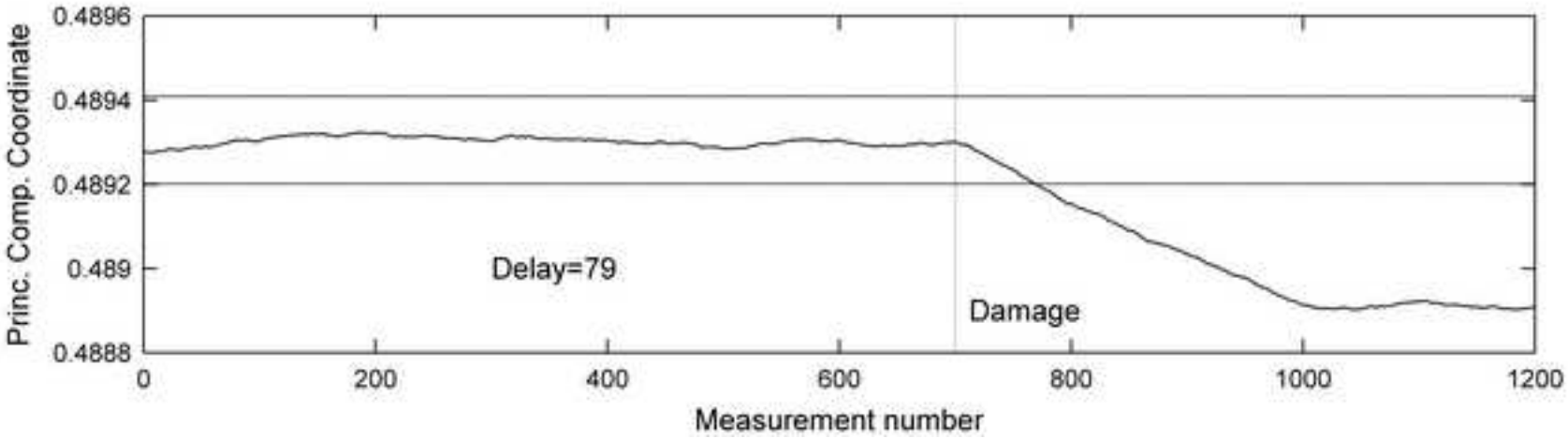

Figure 11

Click here to download high resolution image

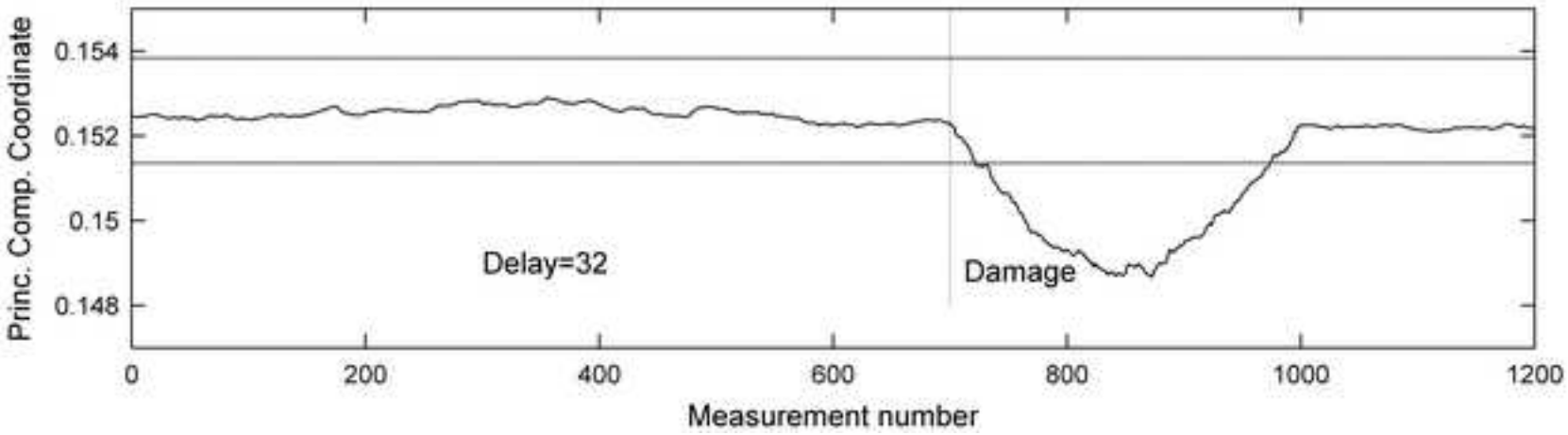

Figure 12.a
Click here to download high resolution image

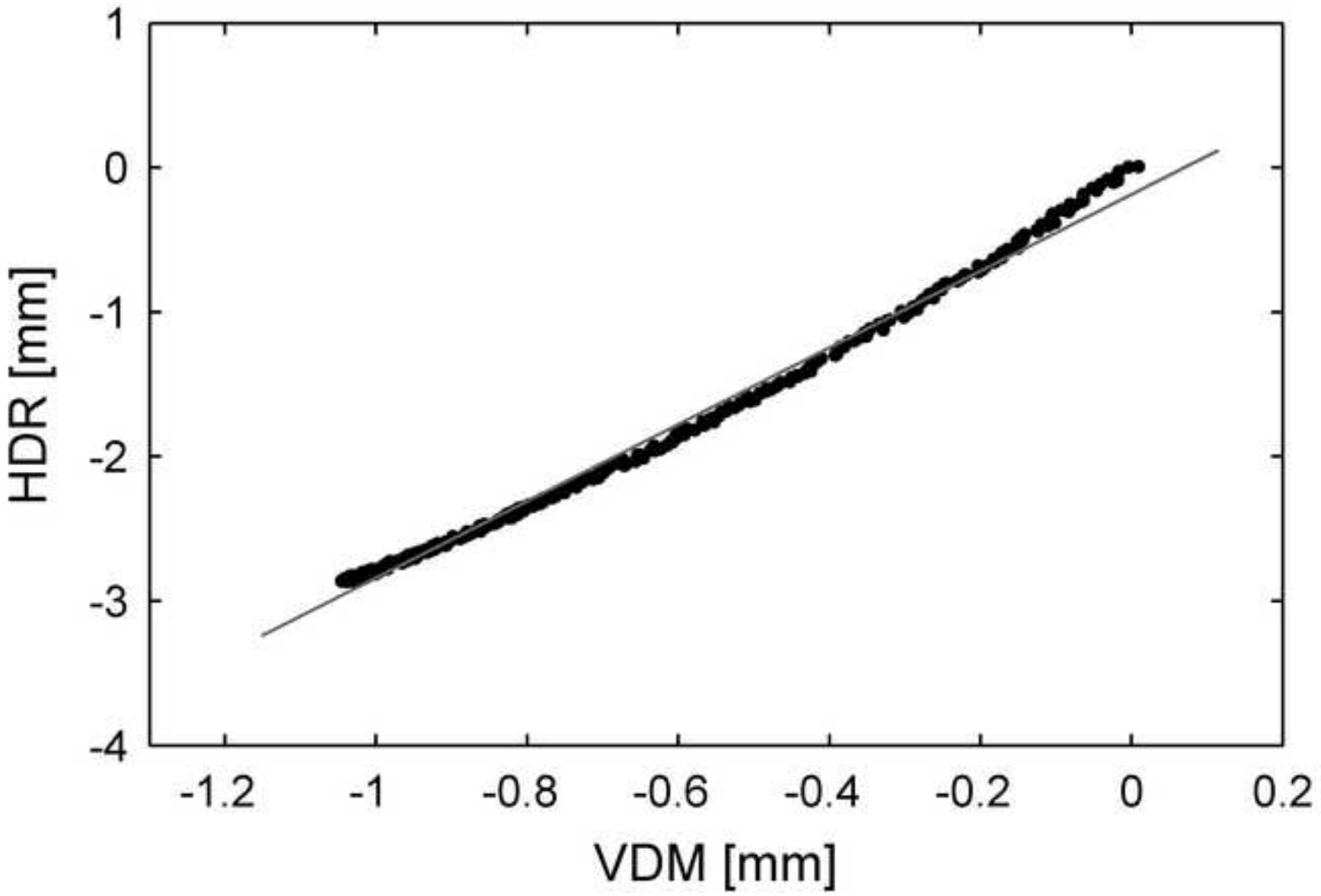

Figure 12.b

Click here to download high resolution image

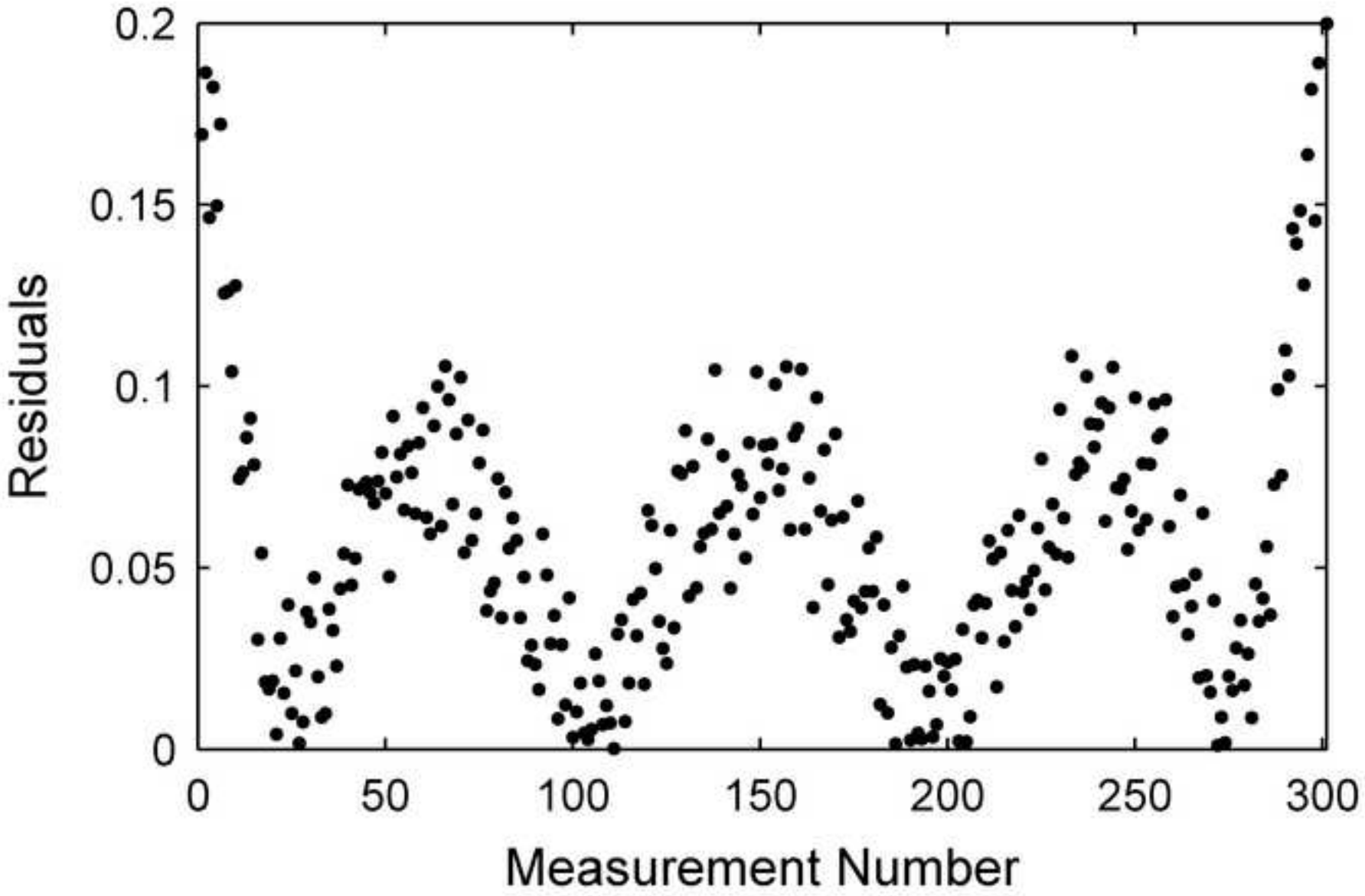

Figure 13.a

Click here to download high resolution image

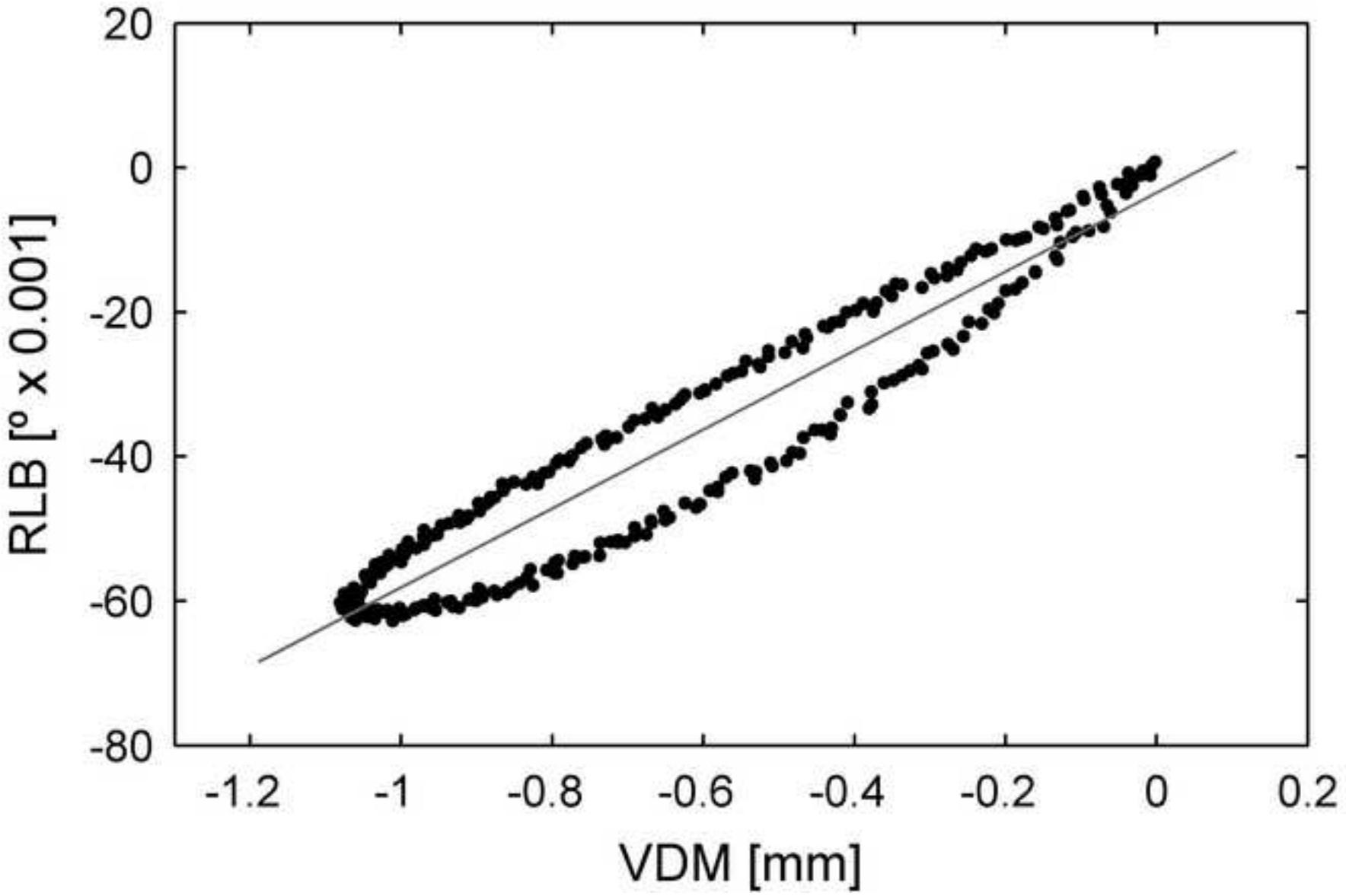

Figure 13.b

Click here to download high resolution image

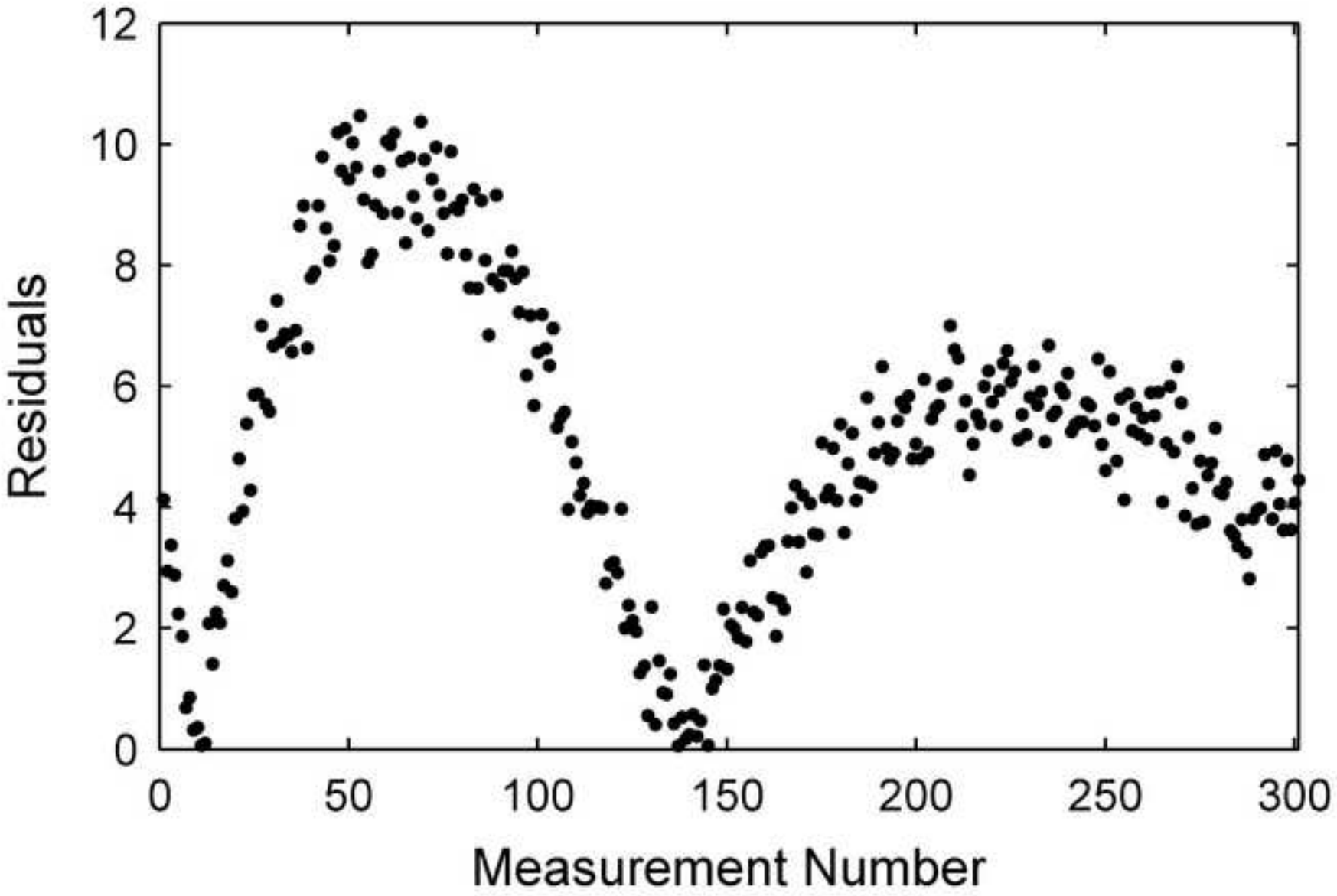

Figure 14.a

Click here to download high resolution image

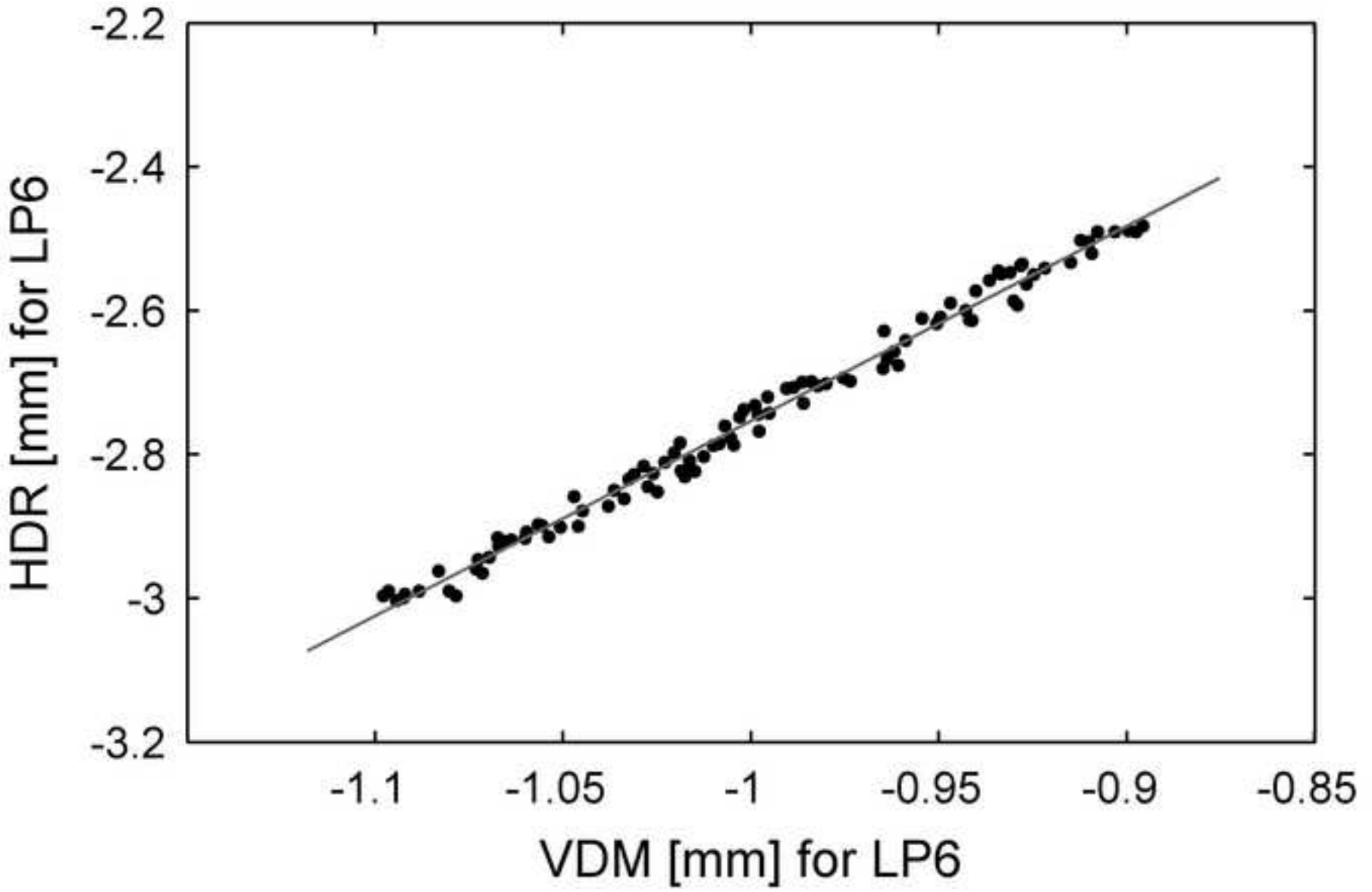

Figure 14.b

Click here to download high resolution image

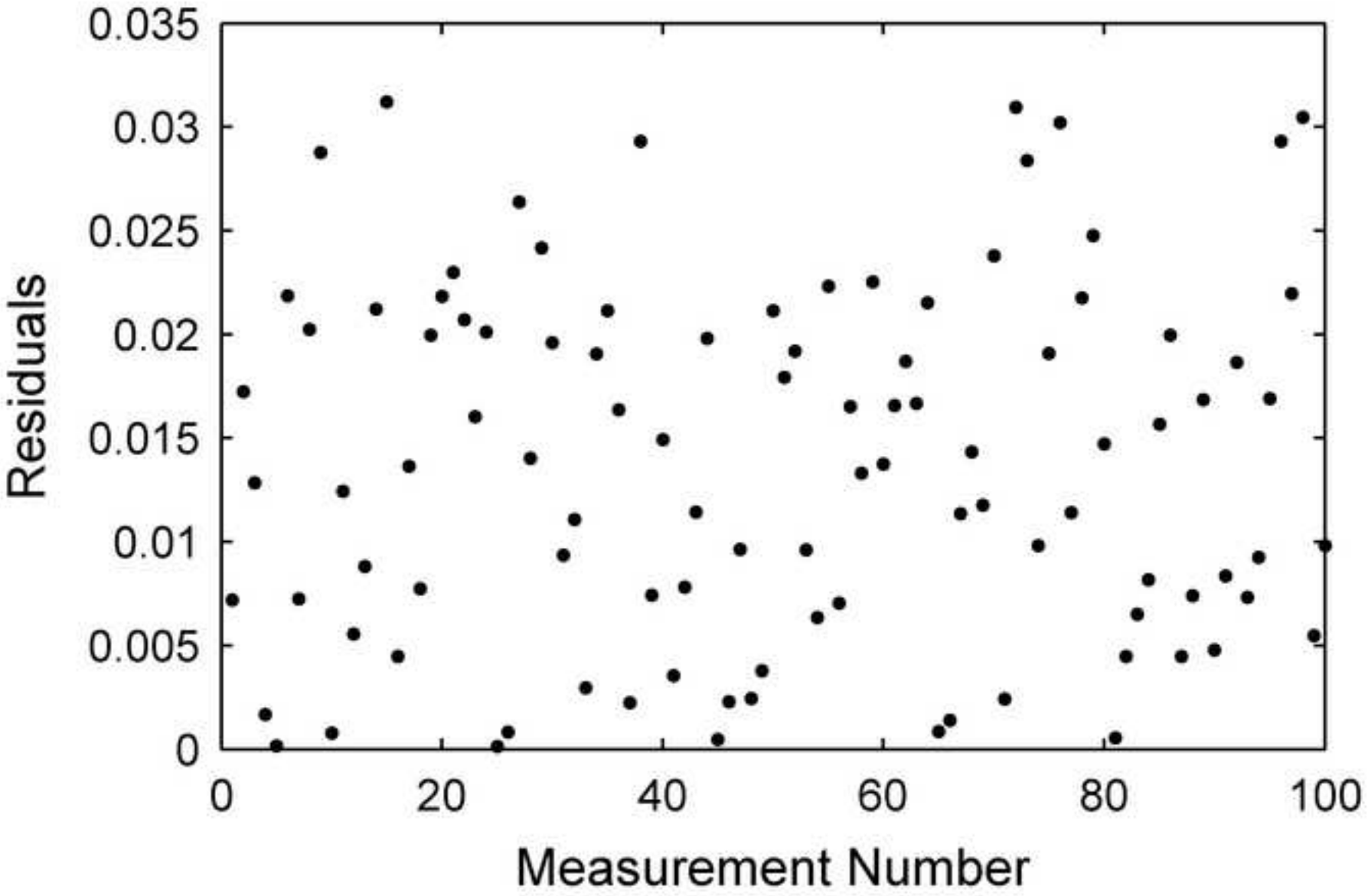

Figure 15

Click here to download high resolution image

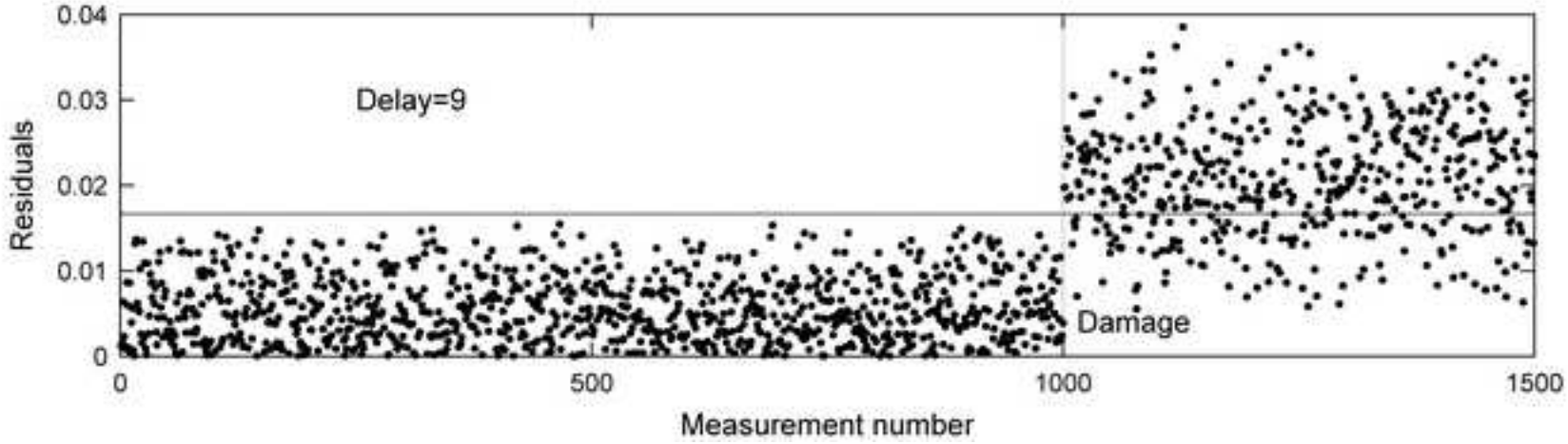

Figure 16

Click here to download high resolution image

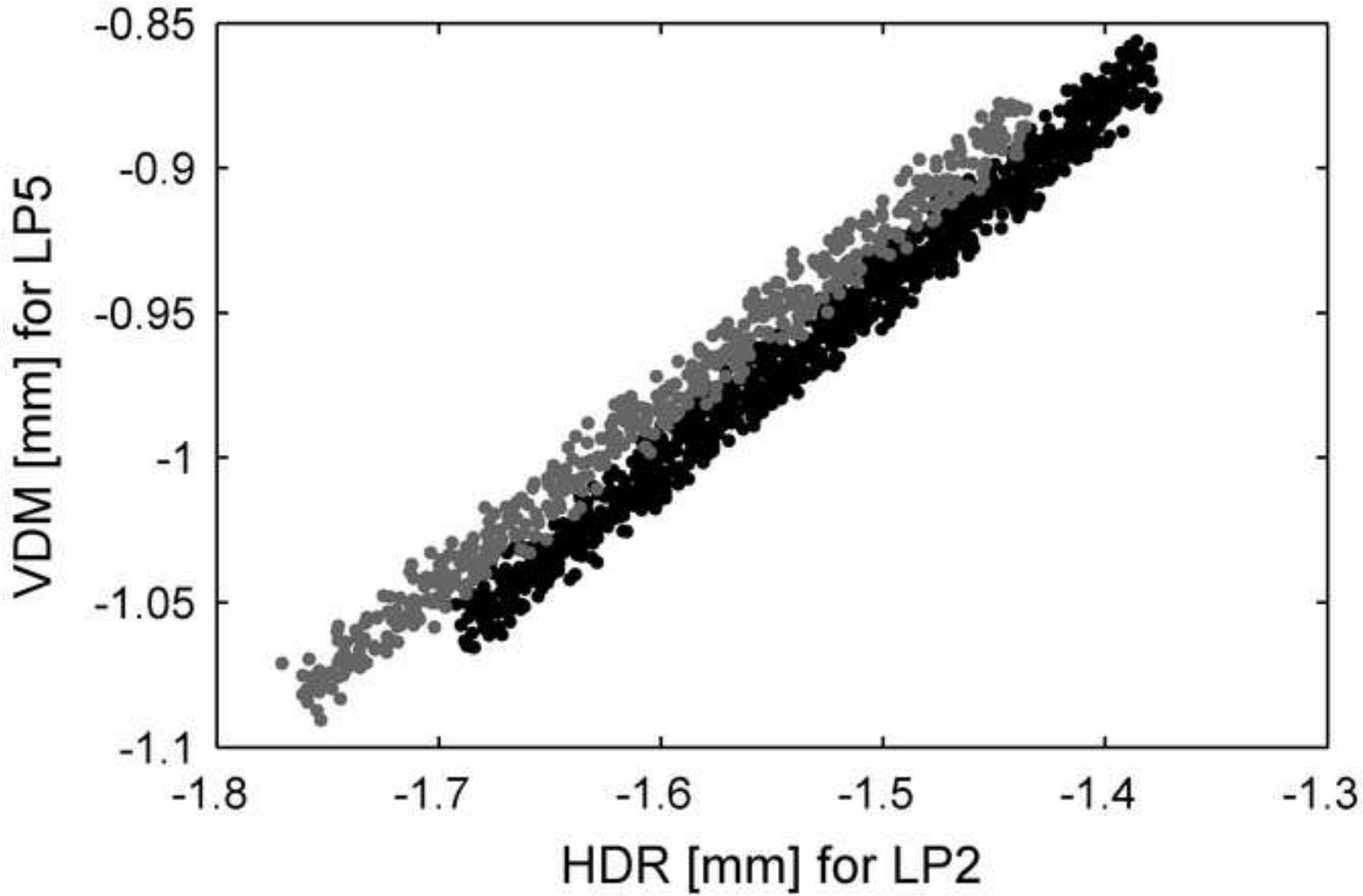

This work is licensed under a Creative Commons Attribution-NonCommercial-NoDerivatives 4.0 International License